JGR Oceans

RESEARCH ARTICLE
10.1029/2025JC022372

Microbial and Metazoan Activity in Monterey Bay, CA Recorded in Nitrogen Isotope Ratios of Sinking and Suspended Particles

S. C. Doherty[1,2], **C. A. Choy**[3], **N. L. Paul**[4], **and H. G. Close**[1]

[1]University of Miami, Rosenstiel School of Marine, Atmospheric, and Earth Science, Miami, FL, USA, [2]University of Alaska Fairbanks, College of Fisheries and Ocean Sciences, Fairbanks, AK, USA, [3]Integrative Oceanography Division, Scripps Institution of Oceanography, University of California San Diego, La Jolla, CA, USA, [4]Interdepartmental Graduate Program in Marine Science, University of California, Santa Barbara, CA, USA

Key Points:

- We examine plankton-particle interactions in three depth zones of Monterey Bay: upper epipelagic, lower epipelagic, and mesopelagic
- Migrating and resident zooplankton leave behind fecal material entrained in suspended particles at their grazing depths
- Much of zooplankton fecal pellet production may be disaggregated and entrained in the epipelagic zone, above the export depth

Correspondence to:
S. C. Doherty,
scdoherty@alaska.edu

Citation:
Doherty, S. C., Choy, C. A., Paul, N. L., & Close, H. G. (2025). Microbial and metazoan activity in Monterey Bay, CA recorded in nitrogen isotope ratios of sinking and suspended particles. *Journal of Geophysical Research: Oceans*, *130*, e2025JC022372. https://doi.org/10.1029/2025JC022372

Received 15 JAN 2025
Accepted 15 SEP 2025

Author Contributions:
Conceptualization: S. C. Doherty, C. A. Choy, H. G. Close
Data curation: S. C. Doherty, N. L. Paul, H. G. Close
Formal analysis: S. C. Doherty, N. L. Paul, H. G. Close
Funding acquisition: C. A. Choy, H. G. Close
Investigation: S. C. Doherty, H. G. Close
Methodology: S. C. Doherty, N. L. Paul, H. G. Close
Project administration: C. A. Choy, H. G. Close
Resources: C. A. Choy, H. G. Close
Supervision: H. G. Close
Validation: S. C. Doherty
Visualization: S. C. Doherty
Writing – original draft: S. C. Doherty, H. G. Close

Abstract Particulate organic matter supports pelagic food webs, and the activity of these food webs attenuates the flux of carbon into the ocean interior. Understanding the extent to which microbial and metazoan heterotrophs influence particle dynamics is essential to describing the biological carbon pump and nutrient delivery to deep ecosystems. We present results of bulk and compound-specific nitrogen stable isotope analyses and a Bayesian mixing model of zooplankton fecal pellets (FP), phytoplankton, and microbial detritus end-members on size-fractionated particulate organic matter from 10 depths in the upper 500 m of Monterey Bay, CA. Our results suggest three distinct zones of plankton-particle interactions in Monterey Bay: primary production and grazing from 0 to 60 m, intense microbial reworking from 60 to 200 m, and inclusion into metazoan food webs below 200 m. Zooplankton FP signatures were found in a <20 μm particle size fraction, both at the approximate depth to which zooplankton migrate at night (~25–60 m) and in the mesopelagic at the approximate depth to which zooplankton migrate during the day (~200 m). This finding indicates that fecal pellets were rapidly disaggregated at the depth at which they were produced, which has implications for estimates of zooplankton FP contribution to carbon export and modeling efforts. In some water columns, much of zooplankton FP production may be disaggregated and entrained in the epipelagic zone, above the export depth.

Plain Language Summary Particles made of organic material feed microbes and zooplankton in the ocean; plankton and microbes in turn contribute to the material in these particles through their cells and feces. We examine how zooplankton and microbes interact with particles, so we can better understand the ocean food web. We split particles into two sizes, small and large, to distinguish between particles that sink (large) from those that do not (small). We use stable isotope ratios of amino acids as a tool to determine how particles interact with microbes and plankton. We use our results to describe three depth zones of plankton and microbe activity in Monterey Bay: a zone of photosynthesis and zooplankton grazing, a zone of elevated microbe activity, and a zone of complex plankton food webs in the "twilight zone." We also found evidence of zooplankton feces in small particles at the same depths plankton visit at night to feed, and thus, zooplankton leave behind a chemical "signature" in particles anywhere they are active. Zooplankton feces, initially large particles, are therefore also likely to be broken up into small particles in the surface ocean instead of sinking to deeper depths.

1. Introduction

Particulate organic matter (POM) in the ocean supports microbial and metazoan plankton food webs, and in turn, these food webs contribute to POM and control its dynamics through remineralization, solubilization, aggregation, and disaggregation (Lam & Marchal, 2015; Steinberg & Landry, 2017). Because sinking POM exports carbon from the surface to the ocean interior and feeds midwater and benthic communities, heterotrophic plankton directly impact ocean carbon sequestration and nutrient delivery to deep ecosystems. Understanding and quantifying the specific relationships between plankton communities and POM is essential to connecting chemical and ecological processes at the ocean surface to those in the interior (Haddock & Choy, 2024).

Metazoan and microbial heterotrophs interact with two distinct pools of POM: suspended or slowly settling particles, which make up most of the POM standing stock, and sinking particles, which make up most of the POM flux. Historically, these two particle groups have been separated by different collection methods, and

Writing – review & editing:
S. C. Doherty, C. A. Choy, N. L. Paul, H. G. Close

compositional distinctions were evident. Suspended particles are often collected via in situ filtration, and sinking particles are often collected in sediment traps (McDonnell et al., 2015). Wakeham and Canuel (1988) found that zooplankton lipid biomarkers dominated in the sediment trap particles in the eastern tropical North Pacific, while suspended particles were dominated by both phytoplankton and zooplankton lipid biomarkers.

More recent work has set a precedent for using size fractions during in situ filtration to separate sinking and suspended particles; sinking particles are represented by the large size fraction (typically >53 or >70 μm), while suspended particles are represented by the small size fraction (often 1–53 or 0.7–53 μm; Lam et al., 2011; Lam & Marchal, 2015). Although the two are not equivalent, the large size class of size-fractionated particles is compositionally similar to particles collected using sediment traps. Abramson et al. (2010) found that fecal pellet (FP) biomarkers (pigments resulting from zooplankton digestion of phytoplankton) appeared in sediment trap and large particle samples and not in small particles in the Mediterranean Sea.

Wojtal et al. (2023) defined three types of particle attenuation processes that result from interactions between plankton and POM: disaggregation, trophic remineralization, and particle solubilization. The authors attributed attenuation in the concentration of size-fractionated particles from the subarctic North Pacific to each of these three processes using signatures from compound-specific nitrogen isotope analysis of amino acids (N CSIA-AA). Disaggregation and consumption/remineralization by zooplankton were the dominant mechanisms for loss of sinking particle flux, and particle solubilization by heterotrophic microbes was the dominant mechanism of particle loss in the suspended particle pool.

Quantifying the interactions between organic matter, heterotrophic microbes, and metazoans can be approached through chemical methods. S. C. Doherty et al. (2021) developed an organic matter end-member framework that included zooplankton fecal pellets and suggested that it would be useful in quantifying the contribution of fecal pellets in particles where morphological identification is not possible, such as the suspended particle pool or morphologically indistinct particles of any size. The end-members were differentiated using the phenylalanine-normalized $\delta^{15}N$ values of alanine and threonine in phytoplankton, microbially degraded organic matter (simplified here to "microbial detritus"), zooplankton fecal pellets, and zooplankton biomass. The $\delta^{15}N$ values of alanine, like those of other trophic amino acids, differentiate consumers from primary producers (e.g., heterotrophic microbial detritus from phytoplankton) and include protistan consumers (Décima et al., 2017; S. C. Doherty et al., 2021; Gutiérrez-Rodríguez et al., 2014). The $\delta^{15}N$ values of threonine differentiate metazoan end-members from microbial end-members (e.g., fecal pellets from phytoplankton and zooplankton from microbial detritus; S. C. Doherty et al., 2021), as threonine fractionation likely occurs during the protein intake and/or gluconeogenesis pathways found in metazoan metabolisms (Fuller & Petzke, 2017). Wojtal et al. (2023) applied these end-members to a Bayesian mixing model to estimate their contribution to size-fractionated particles and sediment traps. The modeled estimates of FP contribution to sediment trap samples were in close agreement with separate estimates from imaging observations (Durkin et al., 2021; Estapa et al., 2021). Therefore, the Bayesian mixing model method allows for a quantitative estimate of microbial and metazoan contributions to both sinking and suspended particle pools.

Both the POM flux and the food web ecology of zooplankton in Monterey Bay, CA have been extensively studied for decades, making this an ideal location to examine the connections between plankton and POM as well as the end-member framework was developed by S. C. Doherty et al. (2021) and applied by Wojtal et al. (2023). Monterey Bay is within the central California Current, an eastern boundary upwelling system. In the summer, equatorward winds along the coast drive water offshore, causing upwelling of deep, cold waters rich in nutrients (Checkley & Barth, 2009). This upwelling of nutrients controls the ecosystem from the bottom-up: periods of high upwelling in Monterey Bay increase animal biomass and/or density from the surface to the benthos (Messié et al., 2023). The bottom-up control is likely mediated by the flux of POM, which connects upwelling-driven diatom blooms to midwater and benthic communities. Diel vertical migrators also connect surface productivity to midwater benthic communities by moving organic matter to depth via their waste and biomass during daily migrations (Haddock & Choy, 2024; Robison et al., 2020). Bathypelagic POM fluxes correspond to upwelling and peak in the summer (Baldwin et al., 1998).

When upwelling relaxes in Monterey Bay, diatom abundance decreases, picophytoplankton abundance increases, and POM flux decreases (Baldwin et al., 1998; Messié et al., 2023). This suggests that the sinking of large particles serves as a seasonal food source to midwater and benthic ecosystems, but these communities may need other food sources for the remainder of the year. In the tropical and subtropical North Pacific, midwater

zooplankton and micronekton have been observed feeding on small particle-based food webs when fluxes of sinking particles are low (Choy et al., 2015; Gloeckler et al., 2018; Hannides et al., 2013, 2020; Romero-Romero et al., 2020). Small particles suspended at depth may similarly serve as a direct or indirect food source to midwater communities in Monterey Bay when POM fluxes are low (e.g., Hetherington et al., 2024). The sampling location for this study, Midwater 1, is a deep water time series site for the study of mesopelagic food webs (Choy et al., 2017; Robison et al., 2010) and is therefore also a good location to examine the role of small and large particles as nutritional sources to midwater consumers.

Here, we investigate the impact of metazoan and microbial plankton on size-fractionated POM by estimating the contributions of zooplankton fecal pellets, microbial detritus, and phytoplankton to size-fractionated particles from depths of approximately 5–500 m in Monterey Bay, CA. Our results are compared to previous studies of plankton dynamics in Monterey Bay to examine the connections between plankton ecology and plankton signatures in POM. Our results highlight the varied and compounding interactions between heterotrophic plankton and POM, with implications for carbon sequestration and midwater ecosystems in Monterey Bay.

2. Materials and Methods

2.1. Particle Collection

Particles were collected from the R/V *Paragon* using in situ filtration pumps (WTS-LV, McLane Research Laboratories) on four consecutive days (31 July–3 August 2017) at three discrete depths per day. Particles were collected at Midwater 1 (MW1; 36.78 N, 122.058 W; 1,600 m total water depth), a mesopelagic time series site in Monterey Bay, CA (for background and history of MW1, see Robison et al., 2017). The three filtration pumps began around 10:00–11:30 each day and ended around 11:30–13:45 for a total pumping duration of 1.5–2.75 hr; pumping duration was longer at deeper sampling depths. The research vessel drifted freely while pumps were deployed. Full details on sampling location and timing can be found with the complete amino acid stable isotope data set (**BCO-DMO**; S. Doherty et al., 2025). Pumps filtered approximately 400–600 L of seawater from each depth. One pump failed to initiate pumping, and filters recovered from this pump were used as full process blanks. Pump depths were determined by temperature-depth loggers attached to pump frames; resulting collection depths were 4.5, 27, 55, 73.5, 100.5, 150, 210.5, 259, 355, and 516 m.

Filters were mounted on mini-MULVFS 3-tiered filter holders, which are designed to exclude swimming zooplankton but include all other, passively sinking particulate material (Bishop et al., 2012). The three size classes were collected using three filters placed on sequential tiers: 100 μm nylon (Nitex) mesh with 150 μm nylon (Nitex) mesh backing, 20 μm nylon (Nitex) mesh with 150 μm nylon (Nitex) mesh backing, and two, stacked 0.7 μm pre-combusted glass microfiber filters (GF/F). The three resulting particle size classes consist of a small particle size class of 0.7–20 μm, an intermediate size class of 20–100 μm, and a large particle size class of >100 μm.

Nitex was pre-cleaned using 10% hydrochloric acid and methanol. After collection, filter holders were stored in a cooler with ice packs frozen at −80°C for two hours until processing in the lab, where filters were photographed, folded, and stored in combusted foil at −80°C until isotopic analysis. The 100 μm nylon (Nitex) filters were split in half, with one half reserved for future analyses.

2.2. CTD Data Collection

Temperature, salinity, and beam attenuation data were collected with a self-recording Seabird Electronics 19plus CTD with WetLabs C-Star transmissometer. The CTD was deployed on the wire below the deepest McLane pump.

2.3. Sample Preparation and Bulk Analysis

Before analysis, particles collected on the 100 μm nylon (Nitex) and 20 μm nylon (Nitex) filters were resuspended in 0.2 μm-filtered seawater in an acid-cleaned plastic bottle with gentle shaking and sonication, then re-filtered onto combusted 47-mm GF/Fs; this process was repeated three times. All filters were lyophilized and inspected under a dissecting microscope (10–40x magnification) to remove Nitex or plastic fibers and whole zooplankton errantly collected. Filters were quantitatively split; approximately 1/16 of the filter was used for elemental analysis and 1/8 to 1/2 of the filter was used for CSIA-AA. Splits used for bulk carbon analysis were treated with

sulfurous acid to remove inorganic carbon. Bulk isotope ratios and carbon and nitrogen masses were determined from the filter splits using a Thermo Scientific Flash Smart elemental analyzer coupled with a MAT 253 isotope ratio mass spectrometer with a Conflo IV interface. Isotope values are reported relative to atmospheric N_2 for nitrogen and Vienna Peedee belemnite (VPDB) for carbon.

The full process blank was found to have no detectable nitrogen but did contain carbon. The carbon quantity and stable isotope ratios associated with GF/F filters was determined for both the 142 mm GF/F (small particles) from the full-process blank and a blank 47 mm GF/F identical to those used to process the large and intermediate particles rinsed with filtered seawater. The filter blank in each sample was estimated using the proportion of total filter used for elemental analysis (fraction weight normalized to total filter weight) and subtracted from the measured carbon. The $\delta^{13}C$ value of each sample was corrected by mass balance as follows:

$$\delta^{13}C_{sample} = \frac{\delta^{13}C_{meas} - X_{filter}\delta^{13}C_{blank}}{(1 - X_{filter})}$$

where X_{filter} is the proportion of the estimated filter blank to the total measured carbon, and $\delta^{13}C_{blank}$ is the $\delta^{13}C$ measured in the filter blanks. After subtracting the filter blank, in most small particle samples, corrected C:N ratios were unreasonably low (e.g., 0.6–2.2), indicating that corrections overestimate the proportion of filter blank. This could be caused by flushing of carbon out of these filters during high-volume in situ filtration, whereas the preparation of intermediate and large particles using 47 mm GF/F filters involved small volumes of seawater. We thus exclude C:N ratios for small particles from this study. Because the measured value of $\delta^{13}C_{blank}$ is close to the range of sample values (−26.8‰) and X_{filter} was low in the epipelagic due to high particle concentrations, we report $\delta^{13}C_{meas}$ values for small particles in the epipelagic zone with a conservative error of 1‰, which encompasses X_{filter} between 0% and 15%. In the deepest intermediate samples, where X_{filter} exceeded 45%, calculated $\delta^{13}C_{sample}$ values were unreasonably higher than the anticipated range of $\delta^{13}C$ values for POM, and thus, we exclude these data as well. Methods for standardization and calculation of concentrations were identical to those described by Wojtal et al. (2023).

2.4. Compound-Specific Nitrogen Stable Isotope Analysis of Amino Acids

Samples estimated to fall below nitrogen amino acid detection limits based on bulk nitrogen measurements and the sample size calculation framework from Close et al. (2019) did not undergo CSIA-AA. Filter splits for CSIA-AA were hydrolyzed to extract amino acids (20 hr at 110°C, 6N hydrochloric acid), purified on cation exchange resin columns (50W-X8, 100–200 mesh) and derivatized to trifluoroacetyl/isopropyl esters for gas chromatography following the methods of Hannides et al. (2013) and identical to S. C. Doherty et al. (2021). The derivatized amino acids were analyzed for nitrogen isotopic composition on a Thermo Trace 1310 gas chromatograph with a BPX5 column (50 m × 0.32 mm, 1.0 μm film thickness) through a combined combustion/reduction interface (Thermo Isolink II, 1,000°C) and liquid nitrogen cold trap, interfaced to a Thermo Conflo IV and MAT 253 isotope ratio mass spectrometer. Three injections were made for each sample where possible, with norleucine and aminoadipic acid with known $\delta^{15}N$ values as coinjection standards. Analytical error for each amino acid $\delta^{15}N$ value was derived from the standard deviation of replicate injections. For some samples, only one injection was obtained due to low particle concentration. For these samples, a conservative uncertainty estimate of 1‰ was assigned. A standard solution of 14 amino acids with known $\delta^{15}N$ values was also analyzed with each set of three injections to track instrument performance, and to correct for instrument drift, including that due to oxidation state of the reactor (Hannides et al., 2013). These same standards, injected in exact quantities, were used to generate response factors for peak area for each amino acid every day. These response factors were then used to calculate relative quantities of amino acids in samples, later used to determine mol% of amino acids. Data from standards injected over the lifetime of the instrument were used to correct for relationships between measured $\delta^{15}N$ values and peak area on the instrument.

2.5. Calculation of $\delta^{15}N_{SrcAA}$, Trophic Position, $\sum V$, and Degradation Index

The average source amino acid $\delta^{15}N$ value ($\delta^{15}N_{SrcAA}$) was calculated by averaging a subset of amino acids (glycine, serine, phenylalanine, and lysine) following Hannides et al. (2020). Estimated trophic position (TP) was

calculated using the $\delta^{15}N$ values of a trophic amino acid (Tr; either glutamic acid + glutamine, Glx, or alanine, Ala) and phenylalanine (Phe) according to the formulation of Chikaraishi et al. (2009):

$$TP = \left(\delta^{15}N_{Tr} - \delta^{15}N_{Phe} - \beta_{Tr-Phe}\right)/\ \Delta_{Tr} + 1 \quad (1)$$

where $\beta_{Glx-Phe}$ is 3.4‰ and Δ_{Glx} is 7.6‰ (Chikaraishi et al., 2009) and $\beta_{Ala-Phe}$ is 3.2‰ and Δ_{Ala} is 6.1‰ (Chikaraishi et al., 2009; Décima et al., 2017). Calculation of propagated uncertainty for TP followed Jarman et al. (2017) and was determined using the standard deviation of β_{Glx}, $\Delta_{Glx-Phe}$, β_{Ala}, and $\Delta_{Ala-Phe}$ from Chikaraishi et al. (2009) (0.9, 1.1, 1.2, and 2.1‰ respectively) and the analytical uncertainty for the amino acid $\delta^{15}N$ of each sample. For Ala-based trophic positions greater than 2, we follow the multi-TDF model (McMahon & McCarthy, 2016) and assume a single protistan step in the food web (Décima et al., 2017; Gutiérrez-Rodríguez et al., 2014) as follows:

$$TP = \left(\delta^{15}N_{Tr} - \delta^{15}N_{Phe} - \beta_{Ala-Phe} - \Delta_{Ala1}\right)/\ \Delta_{Ala2} + 2 \quad (2)$$

where $\beta_{Ala-Phe}$ is the same as above, Δ_{Ala1} is 4.5‰ (Décima et al., 2017), and Δ_{Ala2} is 6.1‰ (Chikaraishi et al., 2009).

The parameter $\sum V$, a proxy for heterotrophic bacterial resynthesis, was calculated following McCarthy et al. (2007) as follows:

$$\sum V = 1/n \sum \left|(\chi_{AA})\right| \quad (3)$$

where n is the number of trophic amino acids. Six trophic AAs were used here: Ala, leucine, isoleucine, proline, aspartic acid, and Glx. χ_{AA} for each of the six amino acids is calculated as follows:

$$\chi_{AA} = \delta^{15}N_{AA} - \delta^{15}N_{TrAA} \quad (4)$$

where $\delta^{15}N_{AA}$ is the $\delta^{15}N$ value of an individual trophic amino acid and $\delta^{15}N_{TrAA}$ is the average $\delta^{15}N$ value of all six trophic amino acids. The propagated analytical error for $\sum V$ was determined by dividing the propagated error for $\delta^{15}N_{TrAA}$ by six or n as described by McCarthy et al. (2007). The degradation index (DI) was calculated relative to the entire data set following Dauwe et al. (1999). The absolute abundance of amino acids (in mol L^{-1}) had high uncertainty in some samples due to small injection volumes, but the relative abundance (mol %) used to calculate DI had high certainty.

2.6. Bayesian Mixing Model

Particles were compared to organic matter end-members from S. C. Doherty et al. (2021) using Phe-normalized $\delta^{15}N$ values of Ala and threonine (Thr). Samples with no Ala and/or no Thr results were excluded from this analysis. A Bayesian mixing model (Markov chain Monte Carlo for stable isotope data with only single target organisms; MixSIAR R package; Stock et al., 2018) was run for particles using three end-members (phytoplankton biomass, fecal pellets, and microbially degraded detritus; excluding zooplankton biomass) and their standard deviations. Mesozooplankton biomass was excluded from the model end-members because particle collection and filter processing methods exclude mesozooplankton biomass; the zooplankton biomass end-member was developed using metazoan mesozooplankton (S. C. Doherty et al., 2021). In contrast, as single-celled microbes, protozoan microzooplankton are captured as a component of POM and can be categorized as heterotrophic microbes. A comparison to cultured protozoan biomass (Gutiérrez-Rodríguez et al., 2014) preliminarily indicates that protozoa should be characterized by the microbial detritus end-member, although further measurements should be conducted to confirm any variations across bacterial and protozoan heterotrophic signatures. Relative contributions of the three end-members were estimated for all particle samples for which CSIA-AA was performed and Ala, Phe, and Thr were successfully measured. The model was run with 500,000 iterations and 50,000 burn-ins, reporting every 10,000 iterations and thinned by 15 iterations.

The posterior distributions of the model for any given sample and end-member often had skewed distributions because end-member proportions are limited to a minimum of 0 and a maximum of 1; when the model converged

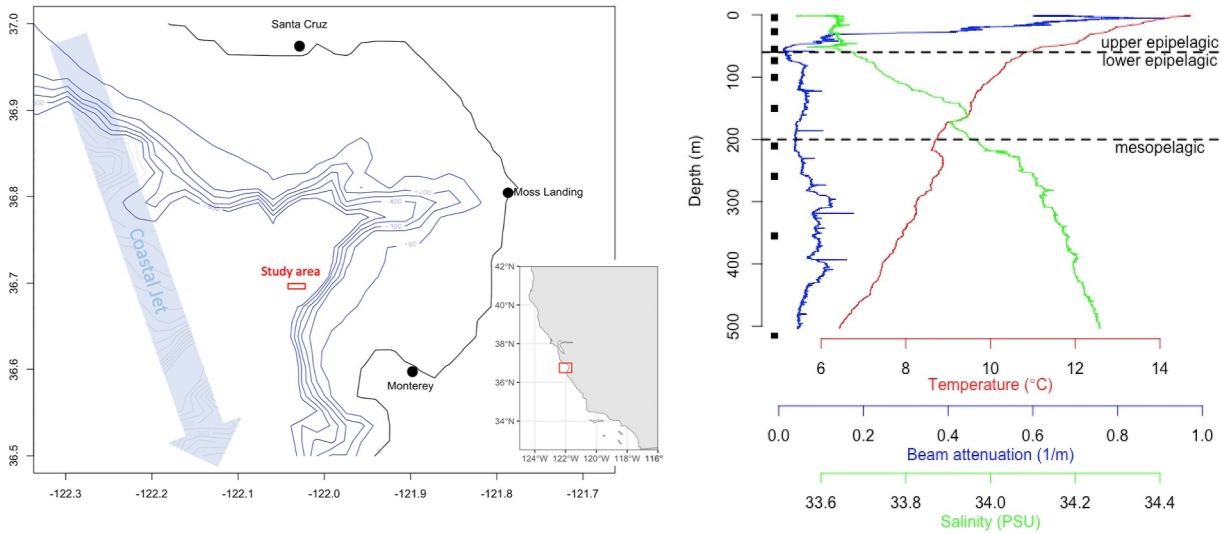

Figure 1. Map of study area in Monterey Bay, with 100 m bathymetric contours (left) and the CTD profile of station Midwater 1 from the first day of particle collection with temperature (degrees Celsius), beam attenuation, and salinity (PSU; right). Division of epipelagic and mesopelagic at 200 m and division of epipelagic into upper and lower zones at 60 m shown by dotted lines. Black squares indicate depths at which particles were sampled. Bathymetric data from NOAA.

on values close to 0 or 1, the posterior distributions were right-skewed or left-skewed, respectively. Therefore, the mean, which has been used previously as a single result of Bayesian mixing models, was not representative of the posterior distributions in these samples. In normal posterior distributions, the mode and mean are approximately equal, but the mean is lower than the mode in left-skewed posterior distributions and higher than the mode in right-skewed posterior distributions. To report a single value result of the posterior distributions, the mode was taken of the reported iterations rounded to two decimal places. The error of the results was determined using the upper- and lower- 75% confidence intervals of the model capped at 100% and 0%, respectively. The average CI was determined by subtracting the mode from the upper and lower 75% confidence intervals, respectively, for each sample, and then taking the mean for all samples.

3. Results

3.1. Hydrographic Setting and Depth Zones

The profile of salinity and temperature (Figure 1) showed that the mixed layer was located at ~60 m. Beam attenuation, a proxy for particle concentration, was highest around 20 m and decreased from 20 to 60 m, below which it remained relatively consistent (Figure 1). In the absence of PAR or fluorescence data to designate the euphotic zone, we divide the epipelagic (0–200 m) into two zones: the "upper epipelagic" from 0 to 60 m, which contains the mixed layer and high beam attenuation expected of phytoplankton production, and the "lower epipelagic" from 60 to 200 m, which contains the upper portions of the halocline and thermocline and consistently low beam attenuation. The upper epipelagic (0–60 m) includes particles collected at 4.5, 27, and 55 m; the lower epipelagic (60–200 m) includes particles collected at 73.5 and 100.5 m; and the mesopelagic (200–1,000 m) includes particles collected at 210.5, 259, 355, and 516 m.

3.2. Bulk Stable Isotope Ratios, C:N Ratios, and Source Amino Acid δ^{15}N Values

At 27 m, all particle size classes had bulk δ^{15}N values of 4.0–6.5‰ ± 0.3‰ (Figure 2, Table 1). The δ^{15}N values increased below 27 m to reach 7.8–8.5‰ ± 0.2‰ (large and intermediate particles) and 10.0‰ ± 0.3‰ (small particles) at 73.5 m depth. With increasing depth below 73.5 m, the bulk δ^{15}N values of large and intermediate particles remained in the range of 7.0–8.5‰, ±0.7‰, with the exception of large particles at 516 m that had a δ^{15}N value of 5.3‰ ± 0.7‰. Below 73.5 m, the bulk δ^{15}N values of small particles were higher, 10.0–11.6‰ ± 0.3‰. In all particles, bulk δ^{13}C values ranged from −24.9 ± 1.0‰ to −18.5 ± 0.2‰ (Table 1). In small particles, bulk δ^{13}C values increased with depth in the epipelagic zone (Figure 2d). In intermediate particles, bulk δ^{13}C values decreased from the epipelagic zone to the mesopelagic zone. In large particles, bulk δ^{13}C values

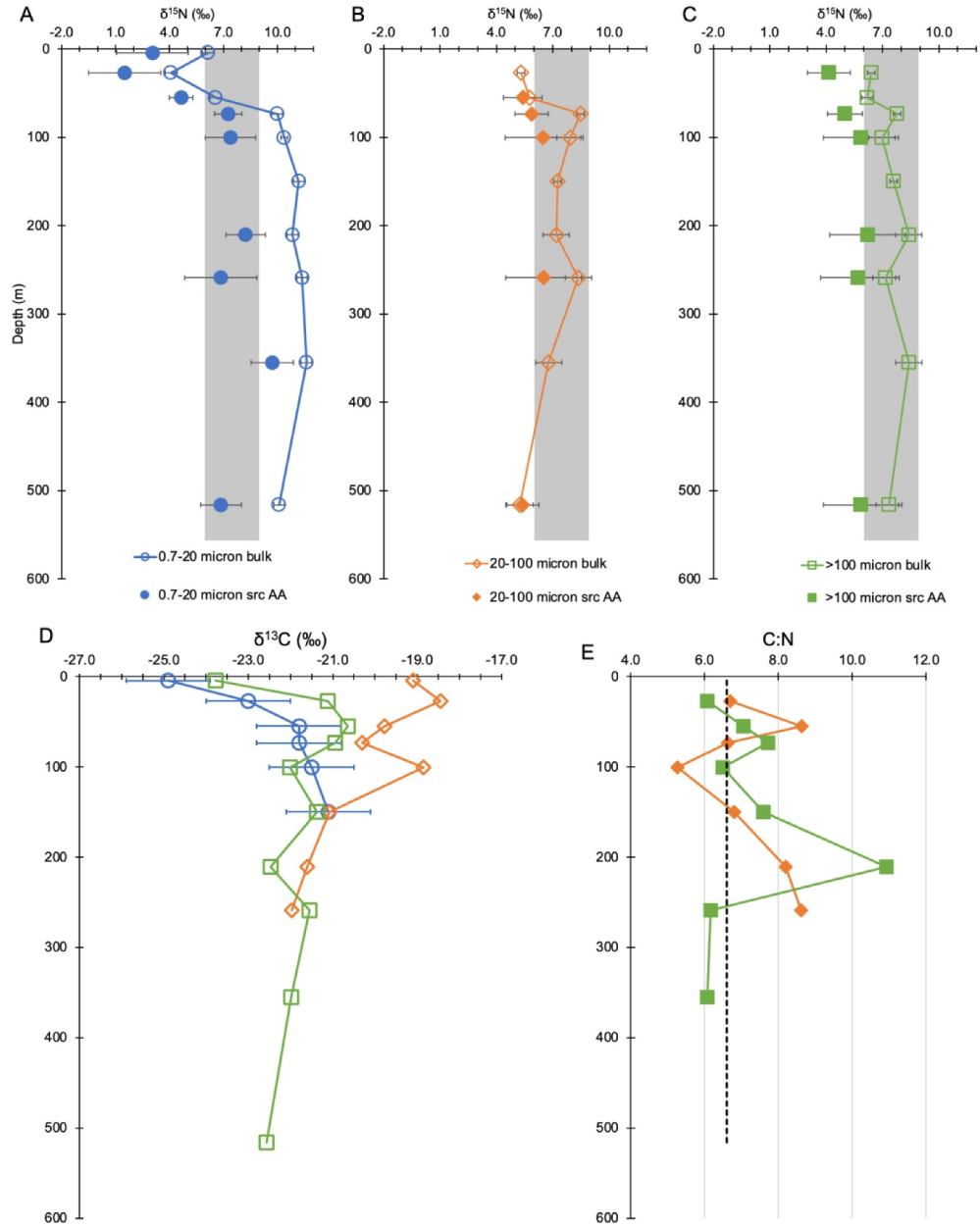

Figure 2. Depth profiles of bulk $\delta^{15}N$ (open symbols connected by lines) and $\delta^{15}N_{SrcAA}$ (solid symbols) in panel (a) small particles (blue, 0.7–20 μm), (b) intermediate particles (orange, 20–100 μm), and (c) large particles (green, >100 μm). Shading represents the $\delta^{15}N$ range of subsurface nitrate in Monterey Bay (Wankel et al., 2007). Depth profiles of bulk $\delta^{13}C$ (d) and C:N ratios (e); the dotted line shows the Redfield C:N ratio 6.6.

were lowest at 4.5 m (−23.7 ± 0.2‰) and varied within 2.0‰ throughout the rest of the water column. C:N ratios in intermediate and large particles ranged from 5.3 to 10.9 (Table 1) and varied with depth (Figure 2e).

The average $\delta^{15}N$ values of the source amino acids ($\delta^{15}N_{SrcAA}$; glycine, serine, Phe, and lysine) were lower than bulk $\delta^{15}N$ values but demonstrated patterns over depth similar to bulk $\delta^{15}N$ values (Figure 2). The bulk $\delta^{15}N$ values and $\delta^{15}N_{SrcAA}$ for all particles were linearly correlated ($R^2 = 0.76$, p-value: 6.7×10^{-7}) with a slope of 1.0 and intercept of 2.0 (Figure 3), indicating that bulk $\delta^{15}N$ values are on average higher by approximately 2‰ than $\delta^{15}N_{SrcAA}$ values. In small particles, $\delta^{15}N_{SrcAA}$ ranged from 1.5 to 4.6‰ ± 2.0‰ in the upper 60 m and from 6.8 to 9.7‰ ± 2.0‰ below 60 m. In large and intermediate particles, $\delta^{15}N_{SrcAA}$ fell within the relatively narrow range of 4.1–6.5‰ ± 2.0‰ at all depths (Table 1, Figure 2).

Table 1
Nitrogen and Carbon Stable Isotope Measurements and Calculated Values for Size-Fractionated Particles Characterized in This Study

Depth (m)	$\delta^{13}C_{bulk}$ (‰)	$\delta^{15}N_{bulk}$ (‰)	$\delta^{15}N_{SrcAA}$ (‰)	Trophic position (Glx-Phe)	Trophic position (Ala-Phe)	∑V (‰)	C:N	DI
Small (0.7–20 μm)								
4.5	−24.9 ± 1.0	6.1 ± 0.3	3.0 ± 2.0	1.0 ± 0.3	1.0 ± 0.5	1.6 ± 0.4	nd	0.28
27	−23.0 ± 1.0	4.1 ± 0.3	1.5 ± 2.0	1.0 ± 0.3	1.0 ± 0.5	1.3 ± 0.4	nd	0.77
55	−21.8 ± 1.0	6.6 ± 0.3	4.6 ± 0.6	1.5 ± 0.2	1.3 ± 0.5	2.0 ± 0.1	nd	−0.16
73.5	−21.8 ± 1.0	10.0 ± 0.3	7.3 ± 0.8	1.3 ± 0.2	1.2 ± 0.5	1.6 ± 0.1	nd	0.13
100.5	−21.5 ± 1.0	10.4 ± 0.3	7.4 ± 1.4	1.5 ± 0.3	1.9 ± 0.7	2.0 ± 0.2	nd	−0.80
150	−21.1 ± 1.0	11.2 ± 0.3	nd	nd	nd	nd	nd	nd
210.5	nd	10.8 ± 0.3	8.2 ± 1.1	2.0 ± 0.3	2.3 ± 0.8	1.7 ± 0.2	nd	−0.34
259	nd	11.4 ± 0.3	6.8 ± 2.0	1.6 ± 0.3	2.5 ± 0.9	2.2 ± 0.4	nd	−0.20
355	nd	11.6 ± 0.3	9.7 ± 1.2	2.0 ± 0.3	2.4 ± 0.8	2.1 ± 0.2	nd	−0.04
516	nd	10.1 ± 0.3	6.9 ± 1.1	1.3 ± 0.3	1.5 ± 0.6	1.6 ± 0.1	nd	−0.43
Intermediate (20–100 μm)								
27	−18.5 ± 0.2	5.3 ± 0.2	nd	1.4 ± 0.3	nd	nd	6.7	−0.50
55	−19.8 ± 0.2	5.8 ± 0.3	5.4 ± 1.0	1.2 ± 0.3	0.9 ± 0.4	2.2 ± 0.2	8.6	−0.11
73.5	−20.3 ± 0.2	8.5 ± 0.2	5.9 ± 0.9	2.0 ± 0.3	3.6 ± 0.8	2.1 ± 0.2	6.6	−0.17
100.5	−18.8 ± 0.2	7.9 ± 0.7	6.5 ± 2.0	1.9 ± 0.3	3.4 ± 0.8	2.0 ± 0.4	5.3	0.39
150	−21.1 ± 0.2	7.3 ± 0.2	nd	nd	nd	nd	6.8	nd
210.5	−21.6 ± 0.2	7.2 ± 0.7	nd	nd	nd	nd	8.2	nd
259	−22.0 ± 0.2	8.4 ± 0.7	6.5 ± 2.0	1.6 ± 0.3	1.7 ± 0.7	1.7 ± 0.4	8.6	−0.35
355	nd	6.8 ± 0.7	nd	nd	nd	nd	nd	nd
516	nd	5.3 ± 0.7	5.4 ± 0.9	1.7 ± 0.3	1.4 ± 0.6	1.6 ± 0.7	nd	−0.48
Large (>100 μm)								
27	−21.1 ± 0.2	6.4 ± 0.2	4.1 ± 1.1	1.5 ± 0.3	1.2 ± 0.5	2.3 ± 0.5	nd	−0.46
55	−20.6 ± 0.2	6.2 ± 0.3	nd	nd	nd	nd	6.1	nd
73.5	−20.9 ± 0.2	7.8 ± 0.2	5.0 ± 0.9	2.1 ± 0.3	3.5 ± 0.8	1.8 ± 0.2	7.0	0.11
100.5	−22.0 ± 0.2	7.0 ± 0.7	5.8 ± 2.0	1.8 ± 0.3	3.4 ± 0.8	1.9 ± 0.4	7.7	0.15
150	−21.4 ± 0.2	7.6 ± 0.2	nd	nd	nd	nd	6.5	nd
210.5	−22.5 ± 0.2	8.4 ± 0.7	6.2 ± 2.0	2.0 ± 0.4	3.4 ± 0.8	1.9 ± 0.4	7.6	0.00
259	−21.5 ± 0.2	7.2 ± 0.7	5.7 ± 2.0	1.3 ± 0.3	1.6 ± 0.6	1.7 ± 0.4	10.9	−0.67
355	−22.0 ± 0.2	8.4 ± 0.7	nd	nd	nd	nd	6.2	nd
516	−22.6 ± 0.2	7.3 ± 0.7	5.9 ± 2.0	1.8 ± 0.3	3.4 ± 0.8	1.9 ± 0.4	6.1	0.38

3.3. Trophic Position, ∑V, and DI

Trophic positions estimated using Glx and Phe (Equation 1) were between 1.0 and 2.1 for all particles, while trophic positions estimated using Ala and Phe were between 0.9 and 3.5 (Table 1). Ala-based trophic positions were within error of Glx-based trophic positions at trophic positions between 1 and 2 but higher than Glx-based trophic positions at trophic positions >2. In small particles, TP was around 1 (primary producer) in the upper 73.5 m (Figure 4a). Below 73.5 m, the TP of small particles was between 1.5 and 2.5. In large and intermediate particles, TP was around 1 in the upper epipelagic and increased to around 3.5 in the lower epipelagic (Figures 4b and 4c). Intermediate particles had trophic positions around 1.5 in the mesopelagic zone (Figure 4b). Large particles in the mesopelagic zone also had trophic positions around 3.5 (Figure 4c), except at 259 m, where they had a lower TP (1.6 ± 0.6).

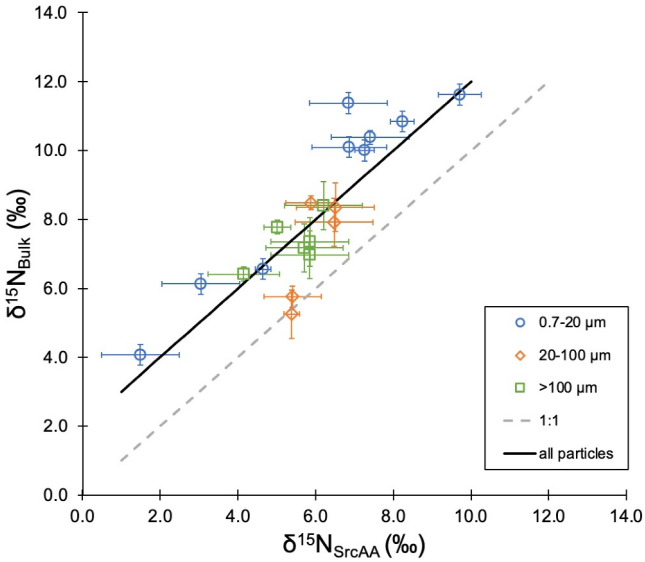

Figure 3. Comparison of bulk $\delta^{15}N$ and $\delta^{15}N_{SrcAA}$ in all particles with a linear fit (solid line) and a 1:1 line for comparison (gray dashed line).

Used here as an estimate of relative microbial resynthesis (McCarthy et al., 2007), ∑V ranged from 1.3 to 2.3 ± 0.4 for all particles (Table 2). In small particles, ∑V values were variable but paralleled relative changes in TP from 4.5 to 100.5 m (Figure 4a). Because of large uncertainties, intermediate and large particles had a similar ∑V value at all depths (Table 1). The amino acid-based degradation index (DI) can be used as an estimate of lability of organic matter, with higher values indicating more labile (less degraded) and lower values indicating less labile (more degraded; Dauwe et al., 1999). DI values are calculated relative to the data set, and thus, these values represent relative lability within this data set. DI values ranged from −0.80 to 0.77, with no consistent depth trend (Table 1, Figure 4d). In small particles, DI decreased from 27 to 100.5 m and increased from 100.5 to 259 m. In intermediate and large particles, DI increased from 27 to 100.5 m.

3.4. Comparison to Alanine-Threonine End-Members

The Phe-normalized values of Ala and Thr for particle samples fell between the FP, microbial detritus, and phytoplankton end-members from S. C. Doherty et al. (2021; Figure 5). No particles fell near the zooplankton biomass end-member. Qualitative groupings in the biplot were primarily by the depth zone and not size class. Upper epipelagic particles generally grouped near the phytoplankton end-member or between the FP and phytoplankton end-members. Lower epipelagic particles generally grouped around the microbial detritus end-member, and mesopelagic particles grouped near the FP end-member. The two exceptions to these general groupings were small particles at 73.5 m, which grouped more closely with the FP end-member, and small particles at 259 m, which grouped more closely with the microbial detritus end-member.

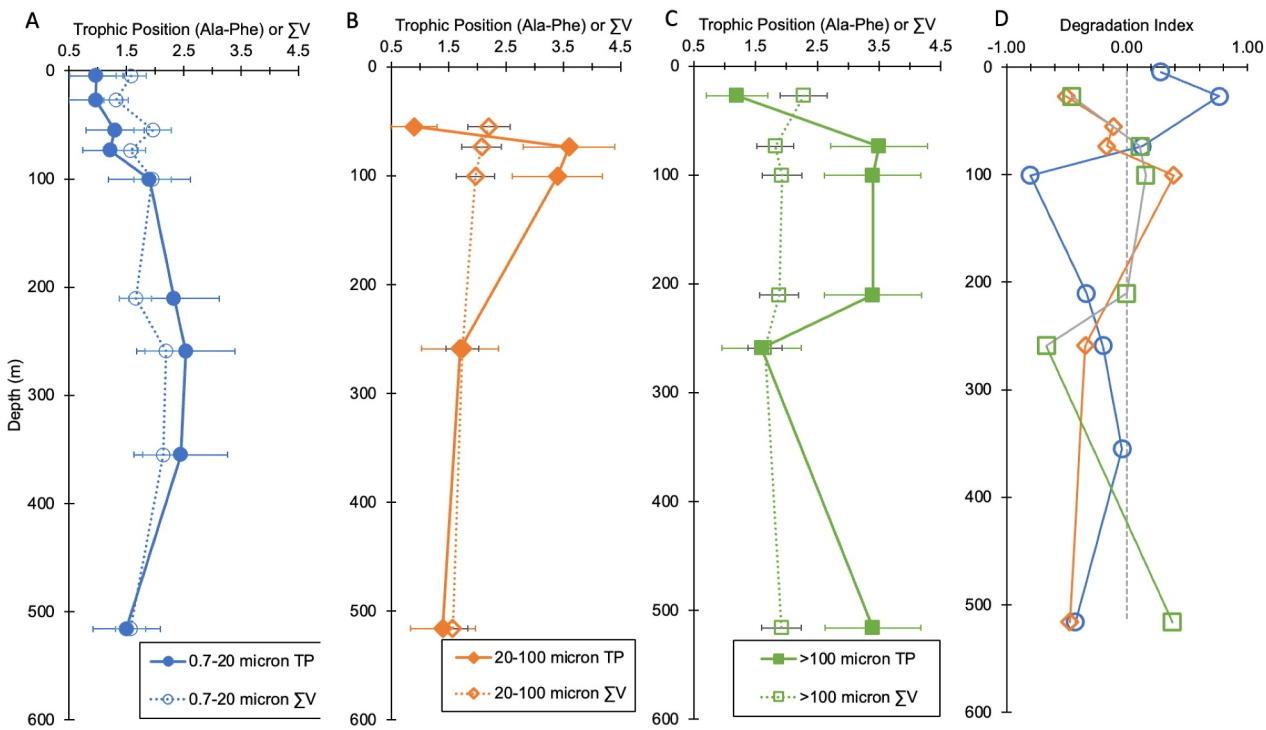

Figure 4. Depth profiles of trophic position calculated using alanine (Ala) and phenylalanine (Phe) (solid symbols) and ∑V (open symbols) in (a) small particles (blue, 0.7–20 μm), (b) intermediate particles (orange, 20–100 μm), and (c) large particles (green, >100 μm). Degradation index values for all particles (d).

Table 2
Bayesian Mixing Model Results for the Proportion of Each End-Member to Size-Fractionated Particles Characterized in This Study

	Proportion fecal pellets			Proportion phytoplankton			Proportion microbial detritus			PN (μg N L^{-1})	
Depth (m)	Mode	Lower 75	Upper 75	Mode	Lower 75	Upper 75	Mode	Lower 75	Upper 75	Total	Est. FP
Small (0.7–20 μm)											
4.5	0.08	0.00	0.59	0.72	0.54	0.95	0.20	0.04	0.53	14.91	1.21
27.0	0.39	0.19	0.63	0.40	0.27	0.56	0.21	0.02	0.35	8.79	3.43
55.0	0.33	0.18	0.58	0.33	0.21	0.48	0.33	0.10	0.45	3.95	1.32
73.5	0.41	0.30	0.75	0.31	0.12	0.45	0.29	0.04	0.38	7.23	2.94
100.5	0.37	0.19	0.62	0.24	0.08	0.38	0.40	0.20	0.59	2.29	0.84
210.5	0.47	0.30	0.84	0.09	0.00	0.25	0.45	0.22	0.66	1.59	0.74
259.0	0.21	0.02	0.66	0.21	0.02	0.41	0.58	0.33	0.91	1.28	0.27
355.0	0.52	0.37	0.91	0.01	0.00	0.18	0.47	0.16	0.62	0.83	0.43
516.0	0.40	0.27	0.72	0.25	0.09	0.41	0.35	0.11	0.49	0.88	0.35
Intermediate (20–100 μm)											
55.0	0.43	0.24	0.72	0.44	0.26	0.57	0.14	0.01	0.33	0.43	0.18
73.5	0.37	0.14	0.66	0.18	0.02	0.33	0.45	0.27	0.76	0.30	0.11
100.5	0.38	0.15	0.63	0.19	0.06	0.38	0.43	0.24	0.69	0.19	0.07
259.0	0.51	0.37	0.87	0.12	0.01	0.29	0.38	0.13	0.54	0.12	0.06
516.0	0.52	0.36	0.83	0.17	0.02	0.30	0.31	0.06	0.42	0.07	0.03
Large (>100 μm)											
27.0	0.01	0.00	0.45	0.61	0.45	0.80	0.38	0.08	0.51	8.37	0.09
73.5	0.16	0.01	0.62	0.32	0.09	0.52	0.52	0.31	0.87	0.59	0.10
100.5	0.31	0.09	0.58	0.29	0.09	0.43	0.40	0.25	0.70	0.33	0.10
210.5	0.56	0.41	0.93	0.01	0.00	0.18	0.43	0.12	0.55	0.28	0.16
259.0	0.48	0.34	0.81	0.17	0.02	0.31	0.35	0.10	0.50	0.13	0.06
516.0	0.46	0.26	0.76	0.09	0.01	0.27	0.45	0.20	0.63	0.25	0.11

Note. The mode, lower 75% confidence interval (CI), and upper 75% confidence interval of posterior distributions are reported. Reported particulate nitrogen (PN) includes measured total PN concentration and estimated fecal pellet (FP) particulate nitrogen concentration from Bayesian mixing model results.

3.5. End-Member Mixing Model

Estimates from the Bayesian mixing model indicate that small particles contained a small proportion of fecal pellets at 4.5 m (8%, 0%–59% CI; Table 2) and moderate to high FP proportions at all other depths (21%–52%, 2%–91% CI). Intermediate particles also contained moderate to high FP proportions (37%–52%, 14%–87% CI) from 55 to 516 m. Fecal pellets contributed a negligible proportion to large particles at 27 m (1%, 0%–45% CI), increasing to a maximum at 210.5 m (56%, 41%–93% CI). Below 210.5 m, approximately half of large particles consisted of fecal pellets (46%–48%, 26%–81% CI).

In all size classes, the modeled phytoplankton (or phytodetritus) contributions decreased with depth in the epipelagic zone (4.5–100.5 m; Table 2). In the mesopelagic zone, modeled phytoplankton contribution decreased further in large particles and were variable in small and intermediate particles. Small particles had a higher estimated contribution of phytoplankton at 516 m than at 355 m (Table 2).

The modeled contribution of microbial detritus to particles was more variable with depth. In all size classes, the lowest estimates of microbial detritus were in the upper 60 m. Microbial detritus was estimated to constitute a fifth of small particles at 4.5 and 27 m (20%–21%, 2%–53% CI). At 55 m and below, the contributions of microbial detritus to small particles were higher and more variable (29%–58%, 4%–91% CI). Intermediate particles had a

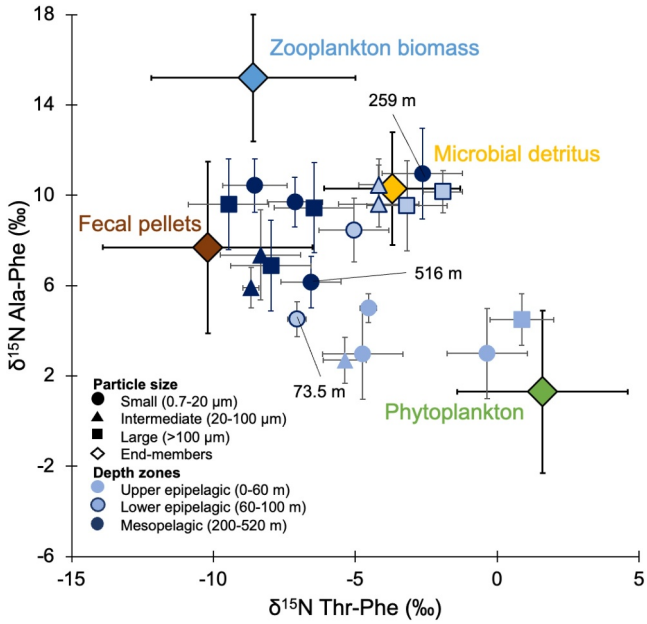

Figure 5. $\delta^{15}N$ values of alanine (Ala) versus threonine (Thr), each normalized to that of phenylalanine (Phe), for particles analyzed here in comparison to organic matter end-members from S. C. Doherty et al. (2021). End-members are labeled diamonds. Symbols for particle data are by particle size classes: small particles (circles, 0.7–20 µm), intermediate particles (triangles, 20–100 µm), and large particles (squares, >100 µm). Colors for particles are by depth range: upper epipelagic (light blue, 0–60 m), lower epipelagic (light blue with dark blue border, 60–200 m), and mesopelagic (dark blue, >200 m). Samples specifically mentioned in Discussion are labeled with depth identification.

similar pattern of estimated microbial detritus contributions with depth. Microbial detritus was estimated as a moderate to high proportion of large particles (35%–52%, 8%–87% CI), with no clear depth trend. The modeled contribution of microbial detritus in all particles has a weak negative correlation with DI (Pearson's correlation coefficient −0.16), a moderate positive correlation with $\sum V$ (Pearson's correlation coefficient 0.39), and a strong positive correlation with $\delta^{15}N_{SrcAA}$ (Pearson's correlation coefficient 0.53). The correlation between modeled microbial detritus and $\delta^{15}N_{SrcAA}$ is especially strong in small particles (Pearson's correlation coefficient 0.74).

3.6. Particulate Nitrogen Concentrations and Estimates of End-Member Concentrations

The particulate nitrogen concentrations of the three particle size classes were highest at the surface and decreased with depth (Table 2). The small (0.7–20 µm) and large (>100 µm) size classes both had similar PN concentrations (8.37 and 8.79 µg N L^{-1}) at 27 m, while the intermediate (0.7–20 µm) size class had a concentration of approximately 0.8 µg N L^{-1} at 27 m. At 55 m, small/suspended (0.7–20 µm) and large (>100 µm) size classes decreased in nitrogen concentration to 3.9 and 1.1 µg N L^{-1}, respectively. The nitrogen concentrations in the intermediate (20–100 µm) size class remained <1 µg L^{-1} below 27 m; and below 55 m, the large (100 µm) size class was comparable to the intermediate size class in concentration. At all depths below 55 m, PN concentrations in the small/suspended (0.7–20 µm) size class were 4–5 times higher than those of the large (>100 µm) size class.

The proportional results from the Bayesian mixing model can be combined with PN concentrations to estimate changes in concentrations of end-member components with depth (Table 2). This method assumes that the amino acid $\delta^{15}N$ patterns reflect total nitrogen, which has been documented in the NE Pacific (Wojtal et al., 2023). Yamaguchi and McCarthy (2018) observed that changes in $\delta^{15}N_{bulk}$ of ultrafiltered POM reflected changes in $\delta^{15}N$ of total hydrolyzable amino acids (THAA). They suggest that this finding is due to degradation processes in the nonamino acid fraction of PN, which is either resistant to acid hydrolysis or undergoes only minor isotope fractionation during degradation. Total hydrolyzable amino acids can constitute 20%–60% of PN, depending on particle composition (Close, 2019). The linear correlation between bulk $\delta^{15}N$ values and $\delta^{15}N_{SrcAA}$ in these particles (Figure 3a) suggests that this assumption holds in Monterey Bay as well; the other nitrogenous compounds in these particles must be in a constant ratio to amino acids for this linear correlation to occur. For simplicity, we assume a conservative ± 20% error for end-member contribution estimates. Generally, depth trends in end-member concentration follow depth trends in total PN concentration (Table 2). One major exception were fecal pellets in large particles, which were estimated to contribute 0.06 ± 0.03 to 0.16 ± 0.06 µg N L^{-1} throughout the water column with no clear depth trend (Table 2, Figure 6). Despite a decreasing PN concentration with depth, the modeled concentration of fecal pellets in large particles was consistent throughout the water column. The highest estimated FP concentration in large particles occurred at 210.5 m (Table 2).

3.7. Summary Statistics

A Kruskal-Wallis rank sum test demonstrated that the bulk $\delta^{15}N$, $\delta^{15}N_{SrcAA}$, TP, FP proportion, phytoplankton proportion, and microbial detritus proportion results were not different among size classes when considering the whole water column (*p*-values: 0.26, 0.34, 0.28, 0.55, 0.72, and 0.50, respectively) but were different among depth zones (*p*-values: 0.014, 0.0066, 0.026, 0.011, 0.00068, and 0.025, respectively). The $\sum V$ parameter was not statistically different among size classes (*p*-value: 0.60) or depth zones (*p*-value: 0.77). Bulk $\delta^{15}N$, $\delta^{15}N_{SrcAA}$, and phytoplankton proportion were different among size fractions when considering the depth zones separately (*p*-values: 0.04, 0.03, and 0.04, respectively), but TP, $\sum V$, phytoplankton proportion, and microbial detritus proportion were not distinct between size classes within a depth zone (*p*-values: 0.16, 0.31, 0.09, and 0.11 respectively).

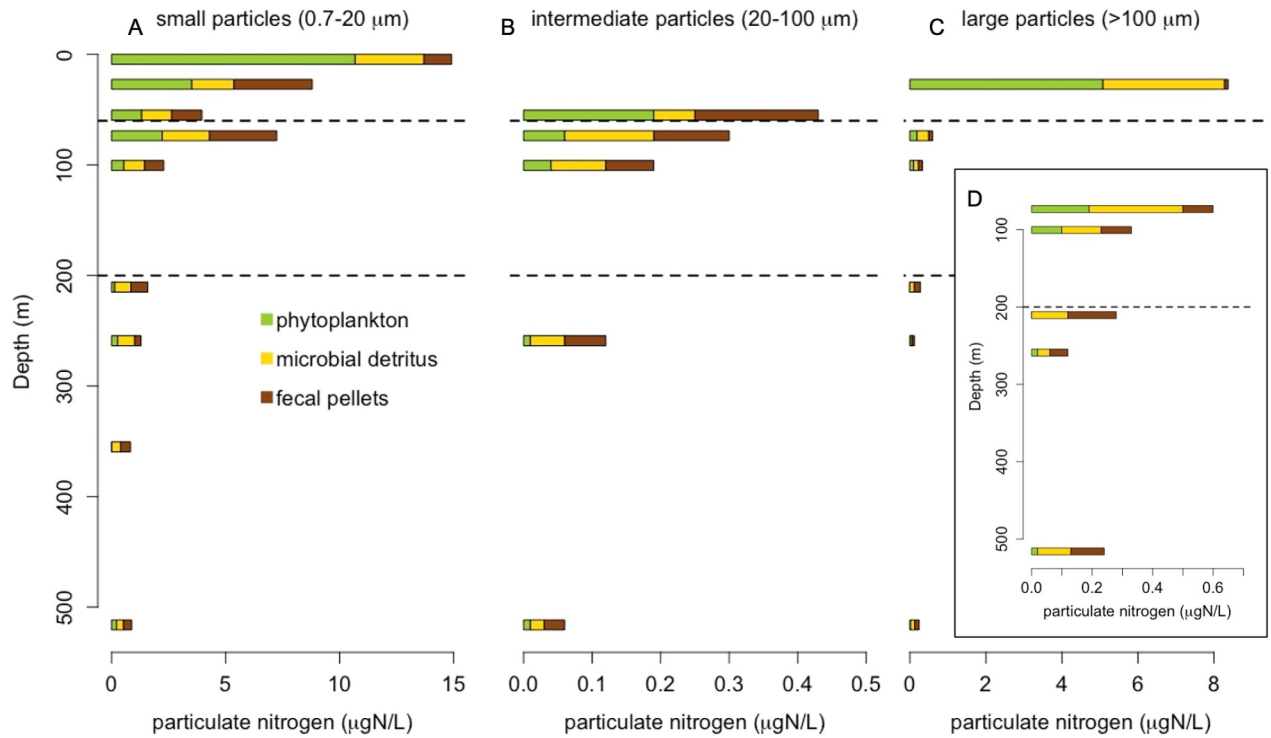

Figure 6. Estimated particulate nitrogen (PN) concentrations deriving from three modeled end-member components: fecal pellets (brown), microbial detritus (yellow), and phytoplankton (green), in panel (a) small particles (0.7–20 μm), (b) intermediate particles (20–100 μm), and (c) large particles (>100 μm). (d) Inset of large particles in lower epipelagic and mesopelagic zones. Dotted lines divide upper epipelagic, lower epipelagic, and mesopelagic zones. The total PN concentration in each panel is equivalent to the measured bulk nitrogen for that size class.

4. Discussion

Our results indicate that the activity of microbial and metazoan heterotrophs along specific depth habitat zones controls POM concentration and composition below the upper epipelagic zone, even in this highly productive system. Clear changes in isotope patterns occurred at similar depths for all particle size classes. Bulk $\delta^{15}N$ values, $\delta^{15}N_{SrcAA}$ values, TP, and the modeled high proportion of phytoplankton and microbial detritus end-members (Tables 1 and 2) differentiated particles in the upper epipelagic zone (0–60 m) from all other depths (pairwise Wilcox rank sum test; p-values: 0.013/0.024, 0.013/0.012, 6.5×10^{-3}, and 0.033, respectively). The estimated high proportion of FP composition differentiated mesopelagic (>200 m) particles from all other depths (pairwise Wilcox rank sum test, *p*-value: 0.024). Bulk $\delta^{15}N$ and $\delta^{15}N_{SrcAA}$ values differentiated small particles in the mesopelagic from intermediate and large particles in the mesopelagic (Figure 2).

The $\delta^{15}N_{SrcAA}$ values in most particles at all depths were linearly correlated with bulk $\delta^{15}N$ values, indicating that changes in bulk $\delta^{15}N$ values were broadly representative of changes to nitrogen sources and microbial solubilization instead of changes in TP (Figure 3). Shen et al. (2021) found similar trends in particles from sediment traps just outside Monterey Bay, in which there was a strong positive linear relationship between bulk $\delta^{15}N$ and $\delta^{15}N_{SrcAA}$.

The modeled phytoplankton proportion differentiated particles in each depth zone from one another (pairwise Wilcox rank sum test; see Table 2 for *p*-values) and generally decreased with depth (Table 2), as would be anticipated from decreasing photoautotroph production with depth. With increasing depth, the proportional contribution from microbial detritus increased in small and intermediate particles, while the proportional contribution from fecal pellets increased with depth in large particles. These relationships suggest that over the entire water column, microbial degradation was dominant in small and intermediate particles. The modeled absolute concentration of nitrogen from fecal pellets in large particles was remarkably consistent throughout the water column (Table 2), indicating that only the relative proportion of fecal pellets increased with depth and not the total concentration of fecal pellets. Wojtal et al. (2023) also found this division in particles from the northeast

Pacific: submicron and 1–6 μm particles were characterized by increasing microbial solubilization with depth, while particles >6 μm and sinking particles were characterized by increasing metazoan signatures with depth.

By examining the depth regions defined above independently, more fine-scale plankton-particle dynamics emerge.

4.1. Upper Epipelagic Particles (0–60 m)

Inorganic nitrogen dynamics likely determined the nitrogen isotope ratios in the upper epipelagic zone. In all particle size classes in the upper epipelagic zone, most bulk $\delta^{15}N$ values were within error of one another and generally fell within the range of both subsurface nitrate in Monterey Bay (~6–9‰; Wankel et al., 2007) and previous studies of PN $\delta^{15}N$ values in Monterey Bay (Rau et al., 1998). As anticipated at the depths where phytoplankton abundance was highest (Dagg et al., 2014), particles in the upper epipelagic zone were modeled as containing the most phytoplankton and the least microbial detritus (Table 2). Small particles had lower $\delta^{15}N$ values at 27 m (upper euphotic zone) than intermediate and large particles (Table 1), a pattern that has been previously observed in other pelagic ecosystems (Altabet, 1988; Gloeckler et al., 2018; Hannides et al., 2020; Rau et al., 1990).

There are at least two potential drivers for the size class differences in $\delta^{15}N$ values near the surface: (a) small particles sink more slowly, so they can entrain a nitrogen source signal from previous weeks or (b) phytoplankton of different sizes were utilizing different inorganic nitrogen sources in Monterey Bay. Rau et al. (1998) found an inverse relationship between nitrate concentration and PN $\delta^{15}N$ values in Monterey Bay; high nitrate concentrations resulted in lower PN $\delta^{15}N$ values. The nitrate concentration at M1 was anomalously high during July 2017 in the weeks leading up to our sampling, and diatom abundance was high (MBARI Monterey Bay Time Series, Chavez & Pitz, 2025). Because small particles are suspended or slowly settling, these particles may have retained some of the previous weeks' high nitrate signal due to a lower $\delta^{15}N$ value. Despite slow sinking speeds, suspended particles would also be turning over quickly due to heterotrophy. Phytoplankton ecology could also explain the differences. Even in oligotrophic environments, smaller phytoplankton sometimes have low $\delta^{15}N$ values consistent with a reliance on recycled nitrogen (ammonium), while larger eukaryotic phytoplankton have higher $\delta^{15}N$ values consistent with subsurface nitrate (Fawcett et al., 2011).

Zooplankton also left behind isotopic signatures in the upper epipelagic zone. Migrating and resident zooplankton graze on phytoplankton in the upper epipelagic zone (Choy et al., 2017; Dagg et al., 2014; Robison et al., 2020) and produce fecal pellets. Dagg et al. (2014) found nighttime maximum abundances of both euphausiids and their fecal pellets around 20 m in Monterey Bay. The production of fecal pellets in the upper epipelagic zone can be considered a mechanism of "biological aggregation," as zooplankton consume small and intermediate particles, which then become packaged into large fecal pellets that sink (Lam & Marchal, 2015). Although we do not directly observe physical aggregation of particles in this analysis, this process likely occurred in the upper epipelagic zone (Cavan et al., 2018; Lam & Marchal, 2015).

It is notable that the largest estimated absolute concentrations of nitrogen from fecal pellets was found in small particles in the upper epipelagic zone (Table 2). Large particles at 27 m were primarily composed of phytoplankton (Figures 5 and 6c), but small and intermediate particles at 27 and 55 m (upper epipelagic) fell between FP and phytoplankton end-members (Figure 5), indicating fecal pellets primarily contribute to smaller particles and not large particles in the upper epipelagic. This finding supports previous hypotheses that disaggregation causes mismatch between FP generation in the euphotic zone and FP export out of the euphotic zone (Stamieszkin et al., 2021; Turner, 2015). Disaggregation may be caused by the feeding behavior of copepods, which often break up fecal pellets prior to ingesting them (Lampitt et al., 1990). The resulting small, suspended particles remain entrained at depth and preserve the signature of zooplankton activity. In a comparison of large particles collected via in situ filtration and neutrally buoyant sediment traps, Wojtal et al. (2023) found that in the northeast Pacific, the proportion of fecal pellets in sediment traps exceeded the proportion in large particles at the same depth, suggesting that large fecal pellets do not remain at a given depth horizon for long. Wojtal et al. (2023), using the same Bayesian mixing model framework presented here, also found FP signatures in suspended particles from the northeast Pacific.

The FP signature in small and intermediate particles in the upper epipelagic zone also may be derived from microzooplankton. Dagg et al. (2014) found maximum ciliate and dinoflagellate concentrations in the upper 50 m

of Monterey Bay. Minipellets, or fecal pellets of microzooplankton (heterotrophic protists and juvenile mesozooplankton), range from 3 to 50 μm (Gowing & Silver, 1985), and therefore would primarily fall in the small and intermediate size classes. However, CSIA-AA signatures have only been established for mesozooplankton fecal pellets and not minipellets (S. C. Doherty et al., 2021).

Future work on contributions of zooplankton fecal pellets to carbon export should consider rates of disaggregation and the dynamics of the suspended particle pool. Combined estimates of particle disaggregation in the epipelagic zone, FP production rates, and FP flux out of the epipelagic zone could be used to better constrain carbon export via fecal pellets in global models.

4.2. Lower Epipelagic Particles (60–100 m)

Heterotrophic microbial activity defined the isotope patterns in the lower epipelagic zone. Almost all particles in the lower epipelagic zone, when plotted on the Ala-Thr end-member biplot from S. C. Doherty et al. (2021), clustered around the microbial detritus end-member (Figure 5). The combination of dramatically attenuating PN concentration (Figure 6) and increasing bulk and source amino acid $\delta^{15}N$ values in the lower epipelagic zone (Figure 2) indicates that microbial degradation was occurring in all size classes over this depth interval (Gloeckler et al., 2018; Hannides et al., 2013, 2020). Between the upper and lower epipelagic zones, both bulk $\delta^{15}N$ and $\delta^{15}N_{SrcAA}$ values increased by ~6‰ in small particles while $\delta^{15}N_{SrcAA}$ values increased by only ~1–2‰ in intermediate and large particles over the same depths. Additionally, $\sum V$, an estimate of relative microbial resynthesis, only increased in small particles and not in intermediate or large particles between the upper and lower epipelagic zones (Table 1). These differences between size classes indicate that small particles underwent more intense bacterial degradation than large or intermediate particles. These size class differences in bulk $\delta^{15}N$, $\delta^{15}N_{SrcAA}$, and/or $\sum V$ have been noted in other pelagic ecosystems (Altabet, 1988; Gloeckler et al., 2018; Hannides et al., 2020) and attributed to more intense microbial solubilization in small particles, which remain suspended in the water column longer and subject to degradation (Hannides et al., 2013).

The correlations between modeled microbial detritus and ΣV and $\delta^{15}N_{SrcAA}$ indicate that our current Bayesian mixing model qualitatively captures changes in microbial contributions for POM. The modeled proportions of microbial detritus in large particles are also similar to estimated microbial contributions to sinking PN from a sediment trap in Monterey Bay (36% ± 14%; Shen et al., 2023), which were made using different methods. However, future applications of the S. C. Doherty et al. (2021) end-members into Bayesian models could be improved by (a) incorporating additional variables into the model to further differentiate end-members and/or (b) measuring the $\delta^{15}N$ values of Thr and Ala in cultured heterotrophic microbial samples and degradation experiments, using environmentally relevant substrates and conditions, to better resolve a microbial biomass and a microbially degraded detritus end-member. Future applications should also consider the best value to summarize Bayesian model posterior distributions when attempting to extract a single modeled proportion value. In some cases, the mode better captures the variability in particle composition, while the mean can obscure the compositional differences between samples.

Wojtal et al. (2023) distinguished the destruction of POM via microbial solubilization, which increases bulk $\delta^{15}N$ and $\delta^{15}N_{SrcAA}$ values of the remaining particulate material, and via trophic remineralization, which increases TP of particles due to the presence of consumer biomass or waste products in the particulate phase. Trophic position increased in all size classes between the upper and lower epipelagic zones (Figure 4). The increase in Glx-based TP between the upper and lower epipelagic zones could indicate an increase in heterotrophic bacterial biomass relative to phytoplankton biomass in particles, as heterotrophic bacteria can have TP dynamics similar to metazoans when they catabolize amino acids (Steffan et al., 2015; Yamaguchi et al., 2017). The closest end-member to microbial consumer biomass in Figure 5 framework is microbial detritus, which the lower epipelagic particles resembled.

A difference in TP estimates based on Ala versus Glx has been used previously to identify protistan contributions to the higher food web, as the Ala-based TP can capture protistan consumers when the Glx-based TP might not (Bode et al., 2021; Décima et al., 2017; Shea et al., 2023). The difference between the two TP estimates at trophic positions >2 suggests that this difference is an effective measure of heterotrophic microbial activity in particles. In the lower epipelagic zone, where other indexes suggest there was more microbial reworking (see above), the difference between the two TP estimates was >1 (Figure 7), indicating a protist (or microzooplankton) step in the food web and/or protist biomass. Interestingly, this additional step is only observed in large and intermediate

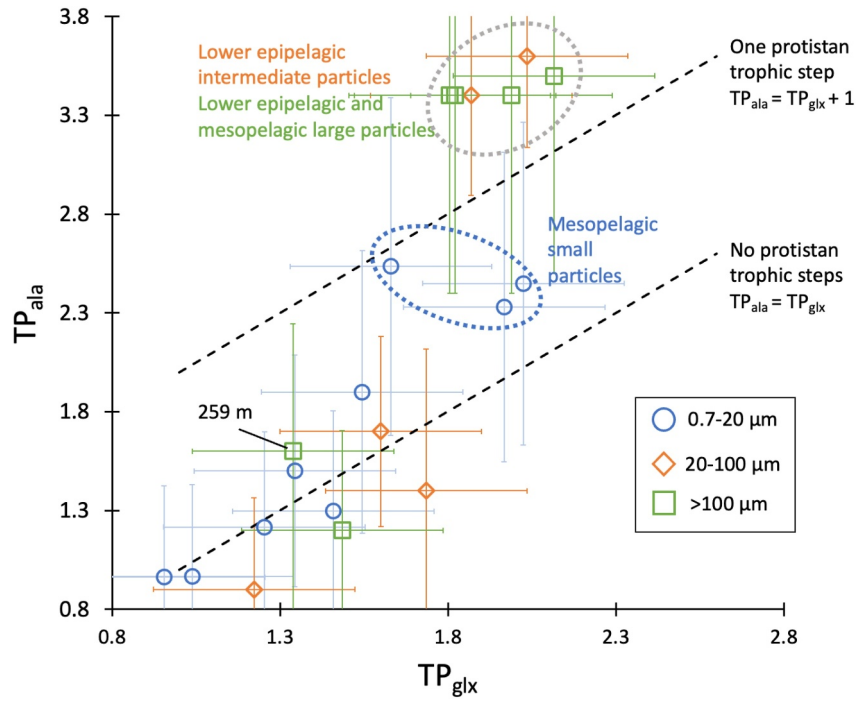

Figure 7. Comparison of Glx-based (TP_{glx}) and Ala-based (TP_{ala}) trophic position calculations for particles. Dotted lines mark no protistan steps in food web ($TP_{ala} = TP_{glx}$) and one protistan step in food web ($TP_{ala} = TP_{glx} + 1$). Nonstatistical groupings of particles are annotated with dotted ellipses.

particles. This may indicate that microbial reworking in small particles primarily derived from heterotrophic bacteria, while in intermediate and large particles, it was due to heterotrophic protists.

In the lower epipelagic depth zone, disaggregation of large particles appeared to both attenuate the flux of large particles and introduce a signature of fecal pellets into the small particle pool. At 73.5 m, small particles group with the FP end-member in Figure 5, resulting in an increase in modeled FP nitrogen in small particles (from 1.32 ± 79 µg N L^{-1} at 55 m to 2.94 ± 1.45 µg N L^{-1} at 73.5 m; Table 2). Considering the rapid disaggregation of fecal pellets in the upper epipelagic likely records the nighttime activity of migrating zooplankton; the increase of an FP contribution to small particles at 73.5 m suggests that this was another feeding depth for zooplankton. Available vertical distribution data from Monterey Bay confirm that zooplankton have migrated to this depth range as well; in addition to a nighttime euphausiid abundance maximum at 20 m, during high flux periods, there was a secondary euphausiid abundance maximum from 70 to 90 m (Dagg et al., 2014). The pelagic red crab, *Pleuroncodes planipes*, also has a nighttime abundance maximum from 50 to 150 m (Choy et al., 2019). Zooplankton activity at this depth also likely causes disaggregation of large particles: The concentration of PN in large particles dropped by more than an order of magnitude between 27 and 73.5 m, while small particle PN concentration increases between 55 and 73.5 m.

4.3. Mesopelagic Particles (200–520 m)

Zooplankton food web dynamics dominated signatures in mesopelagic particles. The $\delta^{15}N$ values of Ala versus Thr for mesopelagic particles almost exclusively grouped with the FP end-member defined by S. C. Doherty et al. (2021; Figure 5). In large particles, the modeled proportion of fecal pellets and FP concentration increased dramatically from 100.5 to 210.5 m (Table 2). The modeled proportion of fecal pellets in small particles also increased to a lesser extent over this depth interval. These FP increases in small and large particles, in addition to trophic positions of 2.0 (Table 1), suggest that 210.5 m is another depth at which there was an injection of zooplankton fecal pellets. During our daytime particle sampling (11:30–13:30 local time), migrating zooplankton would have been located at their mesopelagic migration depth (Dagg et al., 2014). The higher proportion of fecal pellets in large particles is likely due to fecal pellets recently produced by these migrators. Data from the Monterey Bay midwater time series from 1997 to 2015 confirms that the 200–300 m depths were the locations of

highest daytime euphausiid abundance and densities of giant larvaceans *Bathochordaeus* spp. (Robison et al., 2020). Despite the higher modeled proportion of fecal pellets in large particles, small particles still had a higher PN concentration of fecal pellets than large particles at 210.5 m (Table 2), suggesting a buildup of disaggregated fecal pellets over repeated diel migrations. In most particles deeper than 210.5 m, high contributions of fecal pellets (≥40%) were modeled (Table 2), indicating continuing production and disaggregation of fecal pellets in the mesopelagic zone. Lee et al. (2025) also observed zooplankton influence on small and large particles in the eastern tropical North Pacific oxygen deficient zone (ODZ). In those particles, the ODZ determined the depths of zooplankton interactions with particles in the mesopelagic zone.

Horizontal transport of allochthonous POM can also contribute to particles. In this location, allochthonous POM may be most likely in the mesopelagic zone, where resuspended sediments from the shelf may be laterally transported at depth (Hwang & Druffel, 2006; Sherrell et al., 1998). Resuspended sedimentary POM may be recognized by low DI values, high C:N ratios, and trophic positions ~1–1.5 (Batista et al., 2014; Birgit; Dauwe & Middelburg, 1998). These signals are observed in large particles at 259 m, which also have a higher modeled proportion of phytodetritus than large particles at 210.5 m, possibly indicating horizontal advection of sedimentary material. However, the same values could also originate from past phytoplankton flux events. These observations indicate that laterally adveced POM from resuspended sediments may contribute to particles in the mesopelagic zone. The PN concentration in large particles is also higher at 516 m than 259 m, suggesting an injection of PN. This PN could come from laterally advected POM, vertical migrators between 259 and 516 m, or a "pulse" of sinking POM.

Wojtal et al. (2023) not only identified disaggregation of particles by the appearance of large particle (FP) signatures in small particles but also recognized signatures of microbial reworking after disaggregation. Similarly, in this study, small particles at 259 m had a TP and $\delta^{15}N_{SrcAA}$ value similar to those of intermediate and large particles at the same depth (Table 1), but they also showed signs of additional microbial overprinting. Ala and Thr $\delta^{15}N$ values in these particles strongly resembled microbial detritus (Figure 5) and had a higher $\sum V$ than other particles in the mesopelagic zone (Table 1). The estimated trophic positions of these particles also suggest protist contributions (Figure 7). These microbial signatures indicate an increase in microbial activity and/or biomass in small particles at this depth. Mayor et al. (2014) suggested that mesopelagic zooplankton fragment large particles to encourage microbial growth as a feeding strategy referred to as "microbial gardening"; this behavior could account for both the disaggregation and microbial signatures in small particles at 259 m. Below 259 m, small particles resemble fecal pellets (Figure 5), indicating that fecal pellets were disaggregated and incorporated into the small particle pool at these depths. Small particles at 516 m closely resembled small particles at 73.5 m in TP, $\sum V$, position on the Ala-Thr biplot, and modeled end-member composition (Tables 1 and 2, Figure 5). One explanation could be the disaggregation of grazer fecal pellets like those found in small particles in the mesopelagic zone; some of the fecal pellets that sank out of the epipelagic zone may have entered the small particle pool at this depth in the mesopelagic zone.

Small particles can form the base of the mesopelagic food web as a consistent source of nutrition when particle fluxes are low (Gloeckler et al., 2018; Hannides et al., 2020; Romero-Romero et al., 2020). In a study of gelatinous siphonophores, pelagic colonial hydrozoans, Hetherington et al. (2024) suggested that small particles are important dietary sources for the mesopelagic food web in Monterey Bay. Siphonophores collected at mesopelagic depths of Monterey Bay had higher and more variable $\delta^{15}N_{SrcAA}$ values than their epipelagic counterparts, indicating that mesopelagic food webs may utilize a mixture of basal sources: large particles, small particles, and epipelagic particles transported by migrating zooplankton (Hetherington et al., 2024). Therefore, the pool of small, suspended particles at depth must also be considered as a food source when examining mesopelagic food webs.

5. Conclusions

Nitrogen CSIA-AA of size-fractionated particles suggests that there are three distinct zones of plankton-particle interactions in the upper ~500 m of Monterey Bay: an upper epipelagic zone characterized by phytoplankton production and grazing, a lower epipelagic zone characterized by intense microbial reworking of particles, and a mesopelagic zone characterized by interactions between particles and migrating and resident zooplankton food webs (Figure 8). The interpretation presented here represents a snapshot in time of plankton-particle dynamics in the late summer, and these dynamics likely change and shift in depth with the season. Future work in Monterey

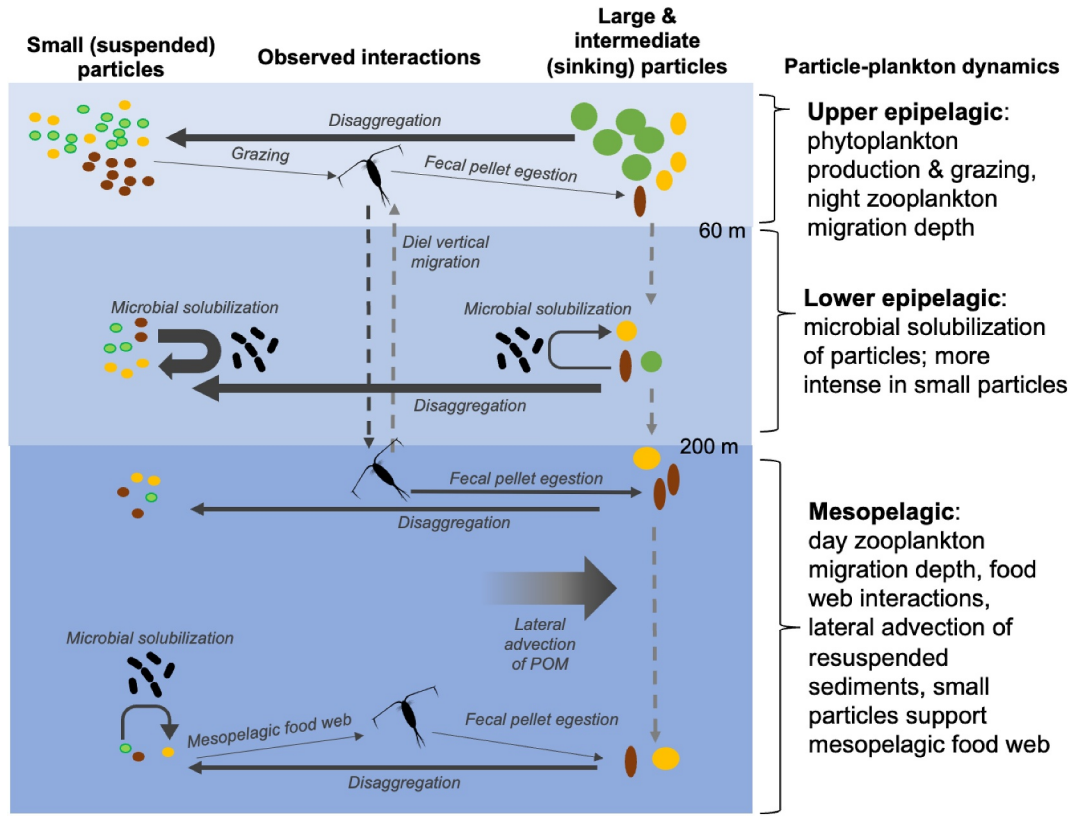

Figure 8. Conceptual snapshot of proposed particle dynamics in Monterey Bay during a higher-flux upwelling regime, based on nitrogen CSIA-AA evidence. Particle colors correspond to composition in Figure 6 (green, phytoplankton; yellow, heterotrophic microbes/microbially degraded; and brown, fecal pellets).

Bay could include repeat particle sampling to describe the changes in plankton-particle dynamics over seasonal cycles and upwelling conditions.

In addition, our results indicate that although zooplankton fecal pellets quickly leave the large particle pool at a given depth through sinking or disaggregation, zooplankton leave behind traces of their activity in the small particle pool, which remains suspended at depth for longer periods of time. Particles collected via in situ filtration, like those presented here, represent a snapshot in time of the water column. If particles are collected at the current depth of the migrating zooplankton community, they will be more likely to contain intact fecal pellets in the large particle size class. If particles are collected after the migrators have left, traces of fecal pellets are more likely to be found only in small particles. Resident zooplankton contribute a consistent concentration of fecal pellets to all depths. The evidence for rapid disaggregation of fecal pellets presented here has implications for estimates of zooplankton FP contribution to carbon export and modeling efforts. Much of zooplankton FP production may be disaggregated and entrained in the epipelagic zone, above the export depth.

Conflict of Interest

The authors declare no conflicts of interest relevant to this study.

Data Availability Statement

All isotopic values and sample information for this study are available through the Biological and Chemical Oceanography Data Management Office (BCO-DMO): https://doi.org/10.26008/1912/bco-dmo.958460.1.

Acknowledgments
We would like to thank Phoebe Lam and Vinicius Amaral, as well as Jared Figurski and Erich Rienecker of MBARI's R/V *Paragon*, who helped facilitate particle sample collection and CTD data retrieval. Albert Ortiz and Josh Pi contributed to stable isotope analysis of particles. This research was supported by NSF OCE-1830016 to H.G.C., NSF OCE-1829812 to C.A.C., the David and Lucille Packard Foundation and L'Oreal For Women in Science Fellowship support to C.A.C., and a Rosenstiel School Student Travel Grant to S.C.D.

References

Abramson, L., Lee, C., Liu, Z., Wakeham, S. G., & Szlosek, J. (2010). Exchange between suspended and sinking particles in the northwest Mediterranean as inferred from the organic composition of in situ pump and sediment trap samples. *Limnology and Oceanography*, *55*, 725–739. https://doi.org/10.4319/lo.2009.55.2.0725

Altabet, M. A. (1988). Variations in nitrogen isotopic composition between sinking and suspended particles: Implications for nitrogen cycling and particle transformation in the open ocean. *Deep-Sea Research, Part A: Oceanographic Research Papers*, *35*(4), 535–554. https://doi.org/10.1016/0198-0149(88)90130-6

Baldwin, R. J., Glatts, R. C., & Smith, K. L. (1998). Particulate matter fluxes into the benthic boundary layer at a long time-series station in the abyssal NE Pacific: Composition and fluxes. *Deep Sea Research Part II: Topical Studies in Oceanography*, *45*(4), 643–665. https://doi.org/10.1016/S0967-0645(97)00097-0

Batista, F. C., Ravelo, A. C., Crusius, J., Casso, M. A., & McCarthy, M. D. (2014). Compound specific amino acid δ^{15}N in marine sediments: A new approach for studies of the marine nitrogen cycle. *Geochimica et Cosmochimica Acta*, *142*, 553–569. https://doi.org/10.1016/j.gca.2014.08.002

Bishop, J. K. B., Lam, P. J., & Wood, T. J. (2012). Getting good particles: Accurate sampling of particles by large volume in-situ filtration. *Limnology and Oceanography: Methods*, *10*, 681–710. https://doi.org/10.4319/lom.2012.10.681

Bode, A., Olivar, M. P., & Hernández-León, S. (2021). Trophic indices for micronektonic fishes reveal their dependence on the microbial system in the North Atlantic. *Scientific Reports*, *11*(1), 8488. https://doi.org/10.1038/s41598-021-87767-x

Cavan, E. L., Giering, S. L. C., Wolff, G. A., Trimmer, M., & Sanders, R. (2018). Alternative particle formation pathways in the Eastern tropical North Pacific's biological carbon pump. *Journal of Geophysical Research: Biogeosciences*, *123*(7), 2198–2211. https://doi.org/10.1029/2018JG004392

Chavez, F. P., & Pitz, K. (2025). Monterey Bay time series data [Dataset]. *MBARI*. https://www.mbari.org/data/mbts-data/

Checkley, D. M., & Barth, J. A. (2009). Patterns and processes in the California current system. *Progress in Oceanography*, *83*(1–4), 49–64. https://doi.org/10.1016/j.pocean.2009.07.028

Chikaraishi, Y., Ogawa, N. O., Kashiyama, Y., Takano, Y., Suga, H., Tomitani, A., et al. (2009). Determination of aquaticfood-web structure based on compound-specific nitrogen isotopic composition of amino acids. *Limnology & Oceanography: Methods*, *7*(11), 740–750. https://doi.org/10.4319/lom.2009.7.740

Choy, C. A., Haddock, S. H. D., & Robison, B. H. (2017). Deep pelagic food web structure as revealed by in Situ feeding observations. *Proceedings of the Royal Society B: Biological Sciences* (Vol. 284(1868), p. 20172116). https://doi.org/10.1098/rspb.2017.2116

Choy, C. A., Popp, B. N., Hannides, C. C. S., & Drazen, J. C. (2015). Trophic structure and food resources of epipelagic and mesopelagic fishes in the North Pacific subtropical Gyre ecosystem inferred from nitrogen isotopic compositions: Trophic structure of pelagic fishes. *Limnology & Oceanography*, *60*(4), 1156–1171. https://doi.org/10.1002/lno.10085

Choy, C. A., Robison, B. H., Gagne, T. O., Erwin, B., Firl, E., Halden, R. U., et al. (2019). The vertical distribution and biological transport of marine microplastics across the epipelagic and mesopelagic water column. *Scientific Reports*, *9*(1), 7843. https://doi.org/10.1038/s41598-019-44117-2

Close, H. G. (2019). Compound-specific isotope geochemistry in the ocean. *Annual Review of Marine Science*, *11*(1), 27–56. https://doi.org/10.1146/annurev-marine-121916-063634

Dagg, M. J., Jackson, G. A., & Checkley, D. M. (2014). The distribution and vertical flux of fecal pellets from large zooplankton in Monterey Bay and coastal California. *Deep-Sea Research Part I Oceanographic Research Papers*, *94*, 72–86. https://doi.org/10.1016/j.dsr.2014.09.001

Dauwe, B., & Middelburg, J. J. (1998). Amino acids and hexosamines as indicators of organic matter degradation state in North Sea sediments. *Limnology & Oceanography*, *43*(5), 782–798. https://doi.org/10.4319/lo.1998.43.5.0782

Dauwe, B., Middelburg, J. J., Herman, P. M. J., & Heip, C. H. R. (1999). Linking diagenetic alteration of amino acids and bulk organic matter reactivity. *Limnology & Oceanography*, *44*(7), 1809–1814. https://doi.org/10.4319/lo.1999.44.7.1809

Décima, M., Landry, M. R., Bradley, C. J., & Fogel, M. L. (2017). Alanine δ^{15}N trophic fractionation in heterotrophic protists. *Limnology & Oceanography*, *62*(5), 2308–2322. https://doi.org/10.1002/lno.10567

Doherty, S., Choy, C. A., Paul, N. L., & Close, H. G. (2025). Compound-specific nitrogen stable isotope ratios of amino acids in size-fractionated particles from Monterey Bay, CA, 2017. *Biological and Chemical Oceanography Data Management Office (BCO-DMO)*. https://doi.org/10.26008/1912/bco-dmo.958460.1

Doherty, S. C., Maas, A. E., Steinberg, D. K., Popp, B. N., & Close, H. G. (2021). Distinguishing zooplankton fecal pellets as a component of the biological pump using compound-specific isotope analysis of amino acids. *Limnology & Oceanography*, *66*(7), 1–15. https://doi.org/10.1002/lno.11793

Durkin, C. A., Buesseler, K. O., Cetinić, I., Estapa, M. L., Kelly, R. P., & Omand, M. (2021). A visual tour of carbon export by sinking particles. *Global Biogeochemical Cycles*, *35*(10), e2021GB006985. https://doi.org/10.1029/2021gb006985

Estapa, M., Buesseler, K., Durkin, C. A., Omand, M., Benitez-Nelson, C. R., Roca-Martí, M., et al. (2021). Biogenic sinking particle fluxes and sediment trap collection efficiency at ocean station papa. *Elementa-Science of the Anthropocene*, *9*(1), 122. https://doi.org/10.1525/elementa.2020.00122

Fawcett, S. E., Lomas, M. W., Casey, J. R., Ward, B. B., & Sigman, D. M. (2011). Assimilation of upwelled nitrate by small eukaryotes in the Sargasso Sea. *Nature Geoscience*, *4*(10), 717–722. https://doi.org/10.1038/ngeo1265

Fuller, B. T., & Petzke, K. J. (2017). The dietary protein paradox and threonine ^{15}N-depletion: Pyridoxal-5'-phosphate enzyme activity as a mechanism for the δ^{15}N trophic level effect. *Rapid Communications in Mass Spectrometry*, *31*(8), 705–718. https://doi.org/10.1002/rcm.7835

Gloeckler, K., Choy, C. A., Hannides, C. C. S., Close, H. G., Goetze, E., Popp, B. N., & Drazen, J. C. (2018). Stable isotope analysis of micronekton around Hawaii reveals suspended particles are an important nutritional source in the lower mesopelagic and upper bathypelagic zones. *Limnology & Oceanography*, *63*(3), 1168–1180. https://doi.org/10.1002/lno.10762

Gowing, M. M., & Silver, M. W. (1985). Minipellets: A new and abundant size class of marine fecal pellets. *Journal of Marine Research*, *43*(2), 395–418. https://doi.org/10.1357/002224085788438676

Gutiérrez-Rodríguez, A., Décima, M., Popp, B. N., & Landry, M. R. (2014). Isotopic invisibility of protozoan trophic steps in marine food webs. *Limnology & Oceanography*, *59*(5), 1590–1598. https://doi.org/10.4319/lo.2014.59.5.1590

Haddock, S. H. D., & Choy, C. A. (2024). Life in the midwater: The ecology of deep pelagic animals. *Annual Review of Marine Science*, *16*(1), 383–416. https://doi.org/10.1146/annurev-marine-031623-095435

Hannides, C. C. S., Popp, B. N., Anela Choy, C., & Drazen, J. C. (2013). Midwater zooplankton and suspended particle dynamics in the North Pacific subtropical Gyre: A stable isotope perspective. *Limnology & Oceanography*, *58*(6), 1931–1936. https://doi.org/10.4319/lo.2013.58.6.1931

Hannides, C. C. S., Popp, B. N., Close, H. G., Benitez-Nelson, C. R., Ka'apu-Lyons, C. A., Gloeckler, K., et al. (2020). Seasonal dynamics of midwater zooplankton and relation to particle cycling in the North Pacific subtropical Gyre. *Progress in Oceanography*, *182*, 102266. https://doi.org/10.1016/j.pocean.2020.102266

Hetherington, E. D., Close, H. G., Haddock, S. H. D., Damian-Serrano, A., Dunn, C. W., Wallsgrove, N. J., et al. (2024). Vertical trophic structure and niche partitioning of gelatinous predators in a pelagic food web: Insights from stable isotopes of siphonophores. *Limnology & Oceanography*, *69*(4), 902–919. https://doi.org/10.1002/lno.12536

Hwang, J., & Druffel, E. R. M. (2006). Carbon isotope ratios of organic compound fractions in oceanic suspended particles. *Geophysical Research Letters*, *33*(23), 1–5. https://doi.org/10.1029/2006GL027928

Jarman, C. L., Larsen, T., Hunt, T., Lipo, C., Solsvik, R., Wallsgrove, N., et al. (2017). Diet of the prehistoric population of Rapa Nui (Easter Island, Chile) shows environmental adaptation and resilience. *American Journal of Physical Anthropology*, *164*(2), 343–361. https://doi.org/10.1002/ajpa.23273

Lam, P. J., Doney, S. C., & Bishop, J. K. B. (2011). The dynamic ocean biological pump: Insights from a global compilation of particulate organic carbon, $CaCO_3$, and opal concentration profiles from the mesopelagic. *Global Biogeochemical Cycles*, *25*(3), 1–14. https://doi.org/10.1029/2010GB003868

Lam, P. J., & Marchal, O. (2015). Insights into particle cycling from thorium and particle data. *Annual Review of Marine Science*, *7*(1), 159–184. https://doi.org/10.1146/annurev-marine-010814-015623

Lampitt, R. S., Noji, T., & von Bodungen, B. (1990). What happens to zooplankton faecal pellets? Implications for material flux. *Marine Biology*, *104*(1), 15–23. https://doi.org/10.1007/BF01313152

Lee, C. W. M., Altabet, M., Mnich, A., & Zhang, L. (2025). Using $\delta^{15}N$ of Amino acids and nitrate to investigate particle production and transformation in the Ocean: A case study from the eastern tropical north Pacific oxygen deficient zone. *Global Biogeochemical Cycles*, *39*(1), e2024GB008280. https://doi.org/10.1029/2024GB008280

Mayor, D. J., Sanders, R., Giering, S. L. C., & Anderson, T. R. (2014). Microbial gardening in the ocean's twilight zone: Detritivorous metazoans benefit from fragmenting, rather than ingesting, sinking detritus: Fragmentation of refractory detritus by zooplankton beneath the euphotic zone stimulates the harvestable production. *Bioessays*, *36*(12), 1132–1137. https://doi.org/10.1002/bies.201400100

McCarthy, M. D., Benner, R., Lee, C., & Fogel, M. L. (2007). Amino acid nitrogen isotopic fractionation patterns as indicators of heterotrophy in plankton, particulate, and dissolved organic matter. *Geochimica et Cosmochimica Acta*, *71*(19), 4727–4744. https://doi.org/10.1016/j.gca.2007.06.061

McDonnell, A. M. P., Lam, P. J., Lamborg, C. H., Buesseler, K. O., Sanders, R., Riley, J. S., et al. (2015). The oceanographic toolbox for the collection of sinking and suspended marine particles. *Progress in Oceanography*, *133*, 17–31. https://doi.org/10.1016/j.pocean.2015.01.007

McMahon, K. W., & McCarthy, M. D. (2016). Embracing variability in amino acid $\delta^{15}N$ fractionation: Mechanisms, implications, and applications for trophic ecology. *Ecosphere*, *7*(12), 1–26. https://doi.org/10.1002/ecs2.1511

Messié, M., Sherlock, R. E., Huffard, C. L., Pennington, J. T., Choy, C. A., Michisaki, R. P., et al. (2023). Coastal upwelling drives ecosystem temporal variability from the surface to the abyssal seafloor. *Proceedings of the National Academy of Sciences* (Vol. 120(13), p. e2214567120). https://doi.org/10.1073/pnas.2214567120

Rau, G. H., Low, C., & Chavez, F. P. (1998). Suspended particle nitrogen Delta ^{15}N versus nitrate ultilization: Observations in Monterey Bay, CA. *Deep-Sea Research*, *45*(8/9), 1603–1616.

Rau, G. H., Teyssie, J. L., Rassoulzadegan, F., & Fowler, S. W. (1990). $^{13}C/^{12}C$ and $^{15}N/^{14}N$ variations among size-fractionated marine particles: Implications for their origin and trophic relationships. *Marine Ecology Progress Series*, *59*, 33–38. https://doi.org/10.3354/meps059033

Robison, B. H., Reisenbichler, K. R., & Sherlock, R. E. (2017). The coevolution of midwater research and ROV technology at MBARI. *Oceanography*, *30*(4), 26–37. https://doi.org/10.5670/oceanog.2017.421

Robison, B. H., Sherlock, R. E., & Reisenbichler, K. R. (2010). The bathypelagic community of Monterey Canyon. *Deep Sea Research Part II: Topical Studies in Oceanography*, *57*(16), 1551–1556. https://doi.org/10.1016/j.dsr2.2010.02.021

Robison, B. H., Sherlock, R. E., Reisenbichler, K. R., & McGill, P. R. (2020). Running the gauntlet: Assessing the threats to vertical migrators. *Frontiers in Marine Science*, *7*(February), 1–10. https://doi.org/10.3389/fmars.2020.00064

Romero-Romero, S., Ka'apu-Lyons, C. A., Umhau, B. P., Benitez-Nelson, C. R., Hannides, C. C. S., Close, H. G., et al. (2020). Deep zooplankton rely on small particles when particle fluxes are low. *Limnology & Oceanography Letters*, *5*(6), 410–416. https://doi.org/10.1002/lol2.10163

Shea, C. H., Wojtal, P. K., Close, H. G., Maas, A. E., Stamieszkin, K., Cope, J. S., et al. (2023). Small particles and heterotrophic protists support the mesopelagic zooplankton food web in the subarctic northeast Pacific Ocean. *Limnology & Oceanography*, *68*(8), 1949–1963. https://doi.org/10.1002/lno.12397

Shen, Y., Guilderson, T. P., Chavez, F. P., & McCarthy, M. D. (2023). Important contribution of bacterial carbon and nitrogen to sinking particle export. *Geophysical Research Letters*, *50*(11), e2022GL102485. https://doi.org/10.1029/2022GL102485

Shen, Y., Guilderson, T. P., Sherwood, O. A., Castro, C. G., Chavez, F. P., & McCarthy, M. D. (2021). Amino acid $\delta^{13}C$ and $\delta^{15}N$ patterns from sediment trap time series and deep-sea corals: Implications for biogeochemical and ecological reconstructions in paleoarchives. *Geochimica et Cosmochimica Acta*, *297*, 288–307. https://doi.org/10.1016/j.gca.2020.12.012

Sherrell, R. M., Paul Field, M., & Gao, Y. (1998). Temporal variability of suspended mass and composition in the Northeast Pacific water column: Relationships to sinking flux and lateral advection. *Deep Sea Research Part II: Topical Studies in Oceanography*, *45*(4), 733–761. https://doi.org/10.1016/S0967-0645(97)00100-8

Stamieszkin, K., Steinberg, D. K., & Maas, A. E. (2021). Fecal pellet production by mesozooplankton in the subarctic Northeast Pacific Ocean. *Limnology & Oceanography*, *9999*(7), 1–13. https://doi.org/10.1002/lno.11774

Steffan, S. A., Chikaraishi, Y., Currie, C. R., Horn, H., Gaines-Day, H. R., Pauli, J. N., et al. (2015). Microbes are trophic analogs of animals. *Proceedings of the National Academy of Sciences* (Vol. 112(49), pp. 15119–15124). https://doi.org/10.1073/pnas.1508782112

Steinberg, D. K., & Landry, M. R. (2017). Zooplankton and the Ocean carbon cycle. *Annual Review of Marine Science*, *9*(1), 413–444. https://doi.org/10.1146/annurev-marine-010814-015924

Stock, B. C., Jackson, A. L., Ward, E. J., Parnell, A. C., Phillips, D. L., & Semmens, B. X. (2018). Analyzing mixing systems using a new generation of Bayesian tracer mixing models. *PeerJ*, *6*, e5096. https://doi.org/10.7717/peerj.5096

Turner, J. T. (2015). Zooplankton fecal pellets, marine snow, phytodetritus and the ocean's biological pump. *Progress in Oceanography*, *130*, 205–248. https://doi.org/10.1016/j.pocean.2014.08.005

Wakeham, G. S., & Canuel, A. E. (1988). Organic geochemistry of particulate matter in the eastern tropical North Pacific Ocean: Implications for particle dynamics. *Journal of Marine Research*, *46*, 183–213.

Wankel, S. D., Kendall, C., Pennington, J. T., Chavez, F. P., & Paytan, A. (2007). Nitrification in the euphotic zone as evidenced by nitrate dual isotopic composition: Observations from Monterey Bay, California. *Global Biogeochemical Cycles*, *21*(2), 1–13. https://doi.org/10.1029/2006GB002723

Wojtal, P. K., Doherty, S. C., Shea, C. H., Popp, B. N., Benitez-Nelson, C. R., Buesseler, K. O., et al. (2023). Deconvolving mechanisms of particle flux attenuation using nitrogen isotope analyses of amino acids. *Limnology & Oceanography*, *68*(9), 1965–1981. https://doi.org/10.1002/lno.12398

Yamaguchi, Y. T., Chikaraishi, Y., Takano, Y., Ogawa, N. O., Imachi, H., Yokoyama, Y., & Ohkouchi, N. (2017). Fractionation of nitrogen isotopes during amino acid metabolism in heterotrophic and chemolithoautotrophic microbes across Eukarya, Bacteria, and Archaea: Effects of nitrogen sources and metabolic pathways. *Organic Geochemistry*, *111*, 101–112. https://doi.org/10.1016/j.orggeochem.2017.04.004

Yamaguchi, Y. T., & McCarthy, M. D. (2018). Sources and transformation of dissolved and particulate organic nitrogen in the North Pacific Subtropical Gyre indicated by compound-specific $\delta^{15}N$ analysis of amino acids. *Geochimica et Cosmochimica Acta*, *220*, 329–347. https://doi.org/10.1016/j.gca.2017.07.036